Neuron

Article

A septal-ventral tegmental area circuit drives exploratory behavior

Graphical abstract

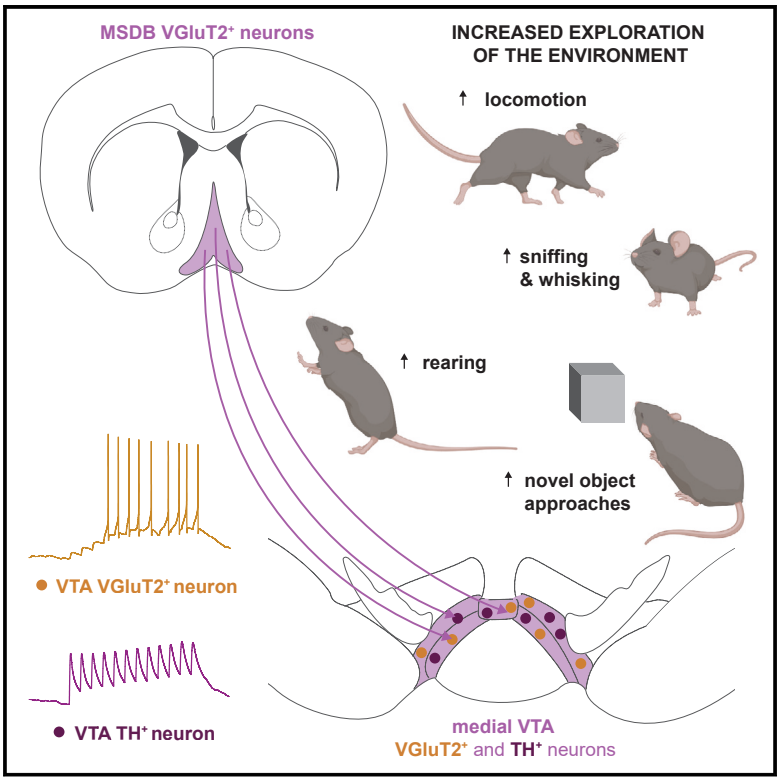

Authors

Petra Mocellin, Oliver Barnstedt, Kevin Luxem, ..., Michael R. Kreutz, Sanja Mikulovic, Stefan Remy

Correspondence

petra.mocellin@lin-magdeburg.de (P.M.), stefan.remy@lin-magdeburg.de (S.R.)

In brief

Mocellin et al. investigate the functional role of the $MSDB_{glu}$ inputs to the VTA. Combining *in vivo* circuit manipulation and *in vitro* electrophysiology, they show that the $MSDB_{glu}$-VTA pathway bidirectionally controls locomotion, increases environmental exploratory actions, and relies on septal inputs to VTA_{DA}, VTA_{glu}, and $VTA_{DA/glu}$ neurons.

Highlights

- $MSDB_{glu}$-VTA circuit bidirectionally controls locomotion
- Activation of the $MSDB_{glu}$-VTA pathway increases exploratory behavior
- $MSDB_{glu}$-VTA-elicited exploration is oriented toward the environment
- $MSDB_{glu}$ axons target VTA_{DA}, VTA_{glu}, and $VTA_{DA/glu}$ neurons

Mocellin et al., 2024, Neuron *112*, 1020–1032
March 20, 2024
https://doi.org/10.1016/j.neuron.2023.12.016

CellPress

CellPress
OPEN ACCESS

Neuron

Article

A septal-ventral tegmental area circuit drives exploratory behavior

Petra Mocellin,[1,2,*] Oliver Barnstedt,[1] Kevin Luxem,[1] Hiroshi Kaneko,[1] Silvia Vieweg,[1] Julia U. Henschke,[1] Dennis Dalügge,[1,2] Falko Fuhrmann,[1] Anna Karpova,[1,4] Janelle M.P. Pakan,[1,3,4] Michael R. Kreutz,[1,3,4,5] Sanja Mikulovic,[1,4,5,6] and Stefan Remy[1,3,4,5,6,7,*]

[1]Leibniz Institute for Neurobiology (LIN), Magdeburg 39118, Germany
[2]International Max Planck Research School for Brain and Behavior (IMPRS), Bonn 53175, Germany
[3]German Center for Neurodegenerative Diseases (DZNE), Magdeburg 39120, Germany
[4]Center for Behavioral Brain Sciences (CBBS), Magdeburg 39106, Germany
[5]German Center for Mental Health (DZPG), Magdeburg 39106, Germany
[6]These authors contributed equally
[7]Lead contact
*Correspondence: petra.mocellin@lin-magdeburg.de (P.M.), stefan.remy@lin-magdeburg.de (S.R.)
https://doi.org/10.1016/j.neuron.2023.12.016

SUMMARY

To survive, animals need to balance their exploratory drive with their need for safety. Subcortical circuits play an important role in initiating and modulating movement based on external demands and the internal state of the animal; however, how motivation and onset of locomotion are regulated remain largely unresolved. Here, we show that a glutamatergic pathway from the medial septum and diagonal band of Broca (MSDB) to the ventral tegmental area (VTA) controls exploratory locomotor behavior in mice. Using a self-supervised machine learning approach, we found an overrepresentation of exploratory actions, such as sniffing, whisking, and rearing, when this projection is optogenetically activated. Mechanistically, this role relies on glutamatergic MSDB projections that monosynaptically target a subset of both glutamatergic and dopaminergic VTA neurons. Taken together, we identified a glutamatergic basal forebrain to midbrain circuit that initiates locomotor activity and contributes to the expression of exploration-associated behavior.

INTRODUCTION

There are multiple reasons for animals to engage in locomotor activity: foraging, fleeing, searching for mates, or exploring the environment.[1] Environmental exploration is necessary for animals to acutely or perspectively satisfy various needs such as food, shelter, or mating. It is expressed as a series of behavioral responses including sniffing, walking, rearing, leaning, jumping, and digging.[2,3] Two different kinds of exploration exist: goal-seeking behavior, which is classically associated with dopaminergic neurotransmission and reward, and information-seeking behavior.[4] The former requires the presence of a cue, or a learned reward site, while in the latter case, the animal moves through an environment, detects salient stimuli, and collects information in the absence of a specific immediate goal. To select appropriate exploratory actions, cortical and subcortical areas continuously integrate internal and external inputs. Among these brain areas, the medial septum and the diagonal band of Broca (MSDB) are in key positions at the interface of the limbic, navigation, and locomotor circuits.[5–10] The MSDB glutamatergic subpopulation ($MSDB_{glu}$) contributes to the spatial representations of the environment by modulating theta oscillations and by conveying speed signals to the hippocampal formation.[7,11] Moreover, $MSDB_{glu}$ neurons play a role both in the detection of salience via habenular projections, as well as in locomotion via the medial basal forebrain bundle.[9] All together, these features identify $MSDB_{glu}$ neurons as an ideal candidate for the neural substrate of exploration. In order to execute this function, $MSDB_{glu}$ neurons must convey information to a downstream region linked to motor and motivational circuits. Tracing studies showed that $MSDB_{glu}$ neurons send input to the ventral tegmental area (VTA),[7,12] a region known for its multiplexed activity underlying motivated behaviors. *In vivo*, VTA neuronal activity is tuned to the animal's position and kinematics[13,14] and sends an acceleration-dependent output to the dorsal striatum,[15] supporting its role in motor execution. VTA neurons increase their activity when novelty and salient stimuli are detected[16,17] and during locomotion in novel environments.[18–20] Thus, we hypothesized that $MSDB_{glu}$ inputs to VTA contribute to motor execution. Indeed, our data demonstrate that the activation of the $MSDB_{glu}$-VTA network reliably induces locomotion and triggers exploration-associated behavior. Moreover, our circuit mapping experiments reveal the monosynaptic nature of the $MSDB_{glu}$-VTA

projections as well as the electrophysiological and molecular profile of the targeted VTA neurons.

RESULTS

$MSDB_{glu}$-VTA circuit mediates locomotion

Activation of $MSDB_{glu}$ neurons evokes locomotion.[7] To investigate if the downstream effects of this neuronal population in motor control are mediated by its projections to the VTA, we injected AAV1-Syn-Flex-GCaMP6s into the MSDB of vesicular glutamate transporter 2 (VGluT2)::Cre mice. Head-fixed mice were allowed to voluntarily move on a linear treadmill while we used fiber photometry to record the activity-dependent Ca^{2+} transients generated by $MSDB_{glu}$ axons in VTA (Figures 1A and S1A–S1C). We observed a consistent increase in $MSDB_{glu}$ axonal activity concurrent with locomotion (Figures 1B–1D). This suggests that $MSDB_{glu}$ axons indeed convey locomotion-related input to VTA. To confirm the causal role of this circuit for locomotion, we specifically activated $MSDB_{glu}$-VTA projections using optogenetics. We injected VGluT2::Cre mice with either an excitatory opsin (AAV1-EF1a-DIO-ChR-EYFP) ($MSDB_{glu}$-VTA:ChR) or an appropriate control construct (AAV1-EF1a-DIO-EYFP) ($MSDB_{glu}$-VTA:EYFP) in the MSDB and used bilaterally implanted optic fibers in the VTA to deliver 473 nm laser light (Figure 1E). Activation of $MSDB_{glu}$-VTA projections along the theta-frequency range (3, 6, 9, and 12 Hz) reliably initiated and maintained locomotion in $MSDB_{glu}$-VTA:ChR-injected animals (Figures 1F and 1G). To exclude the possibility of retrograde action potential propagation after optogenetic stimulation,[21,22] we next silenced the MSDB with lidocaine, a Na^+ channel blocker, while optogenetically driving $MSDB_{glu}$ axons in VTA (Figures S1D–S1F and S2). It has been previously reported that infusion of lidocaine in MSDB significantly reduces hippocampal theta amplitude.[8] Thus, we also simultaneously performed local field potentials (LFPs) recordings in the hippocampus (HPC) as a readout of the effective silencing of septal neurons (Figures 1H and 1I). Indeed, lidocaine injection in the MSDB significantly reduced hippocampal theta amplitude compared with the control saline injection (Figures S3A and S3B). Despite septal inactivation, optogenetic stimulation of $MSDB_{glu}$-VTA axons was sufficient to induce locomotion (Figure 1J). The reliability, mean and maximum speed, and the latency of locomotion onset were not significantly altered after lidocaine injection in the MSDB (Figures S3C–S3F), providing strong evidence that the VTA is a downstream target of the locomotor response initiated by the $MSDB_{glu}$ neurons.

Because the VTA has classically been studied in relation to reward prediction[23] and goal-related behavior,[24] we next tested whether the observed locomotor response was reward oriented. To this end, we trained the animals in a location-specific reward learning task (Figures S4A and S4B). After the mice successfully learned the reward location, we optogenetically stimulated the $MSDB_{glu}$-VTA circuit in both the learned reward zone and in a second zone that was not linked to any reward. Our findings reveal that stimulating the $MSDB_{glu}$-VTA pathway did not significantly impact licking behavior or the ability for mice to encode rewards, and it was not intrinsically rewarding. This was demonstrated by no change in the effective reward consumption at the designated reward location (Figures S4C–S4E) and by the absence of licking behavior when optogenetic stimulation was applied in the non-rewarding zone (Figures S4F and S4G). Thus, these results indicate that the VTA is a direct downstream target of the $MSDB_{glu}$ neuron-driven pathway that is responsible for locomotor activity but not directly linked to reward.

$MSDB_{glu}$-VTA activation increases sniffing and whisking behaviors preceding movement

Information-seeking exploration in mice is typically associated with specific behaviors such as sniffing and whisking.[25] To investigate the contribution of the $MSDB_{glu}$-VTA pathway to exploratory behavior, we monitored the facial dynamics of the animals by applying optical flow detection to high-speed near-infrared camera recordings. We automatically segmented nose and whisker pad regions using markerless pose estimation (DeepLabCut[26]) and quantified the average movement magnitude for these facial regions as proxies for the animals' sniffing and whisking activities[27] (Figure 2A; Video S1). Strikingly, optogenetic stimulation triggered immediate sniffing and whisking behaviors in $MSDB_{glu}$-VTA:ChR mice that preceded locomotion onsets by about 0.5 s, comparable to that of spontaneous behavior (Figures 2B–2D). This increase in facial movement was unaffected by lidocaine injection in the MSDB (Figures 2E–2H). Thus, our data support a role for the $MSDB_{glu}$-VTA network not only in locomotion onset but also in activity related to exploratory behavior.

$MSDB_{glu}$-VTA pathway drives exploratory actions in freely moving mice

Head-fixed experiments may limit behavioral expression. Thus, we sought to determine the effect of stimulation of the $MSDB_{glu}$-VTA projection in mice moving freely in an open-field arena. We optogenetically activated $MSDB_{glu}$-VTA axons using 9 Hz theta stimulation while continuously video monitoring the movement of the animals from a bottom-view camera. Mice exhibited an increase in locomotion and speed in the open-field condition upon activation of the circuit (Figures 3A and 3B). This locomotor effect continued even after we successfully inactivated the action potential firing of neurons in the MSDB using lidocaine (Figures S5A–S5C), confirmed by a reduction in hippocampal theta activity (Figures S5D–S5G). We next applied variational animal motion embedding (VAME)[28] to investigate and segment animal behavior. Using this approach, we analyzed the visible behavioral repertoire with sub-second resolution, classified it into individual behavioral motifs, and clustered them into communities. VAME identified 35 motifs that were hierarchically organized into three non-stationary (run, rear, and walk) and three stationary (sniff, groom, and rest) communities (Figures 3C and 3D; Video S2). The increase in locomotion was reflected by a consistent increase in the prevalence of running motifs. Interestingly, we also observed a significant increase in the prevalence of rearing during stimulation, while resting motifs were nearly absent (Figure 3C). This indicates that the optogenetic activation of $MSDB_{glu}$-VTA inputs is sufficient to evoke not only locomotion but also actions traditionally linked with exploration.

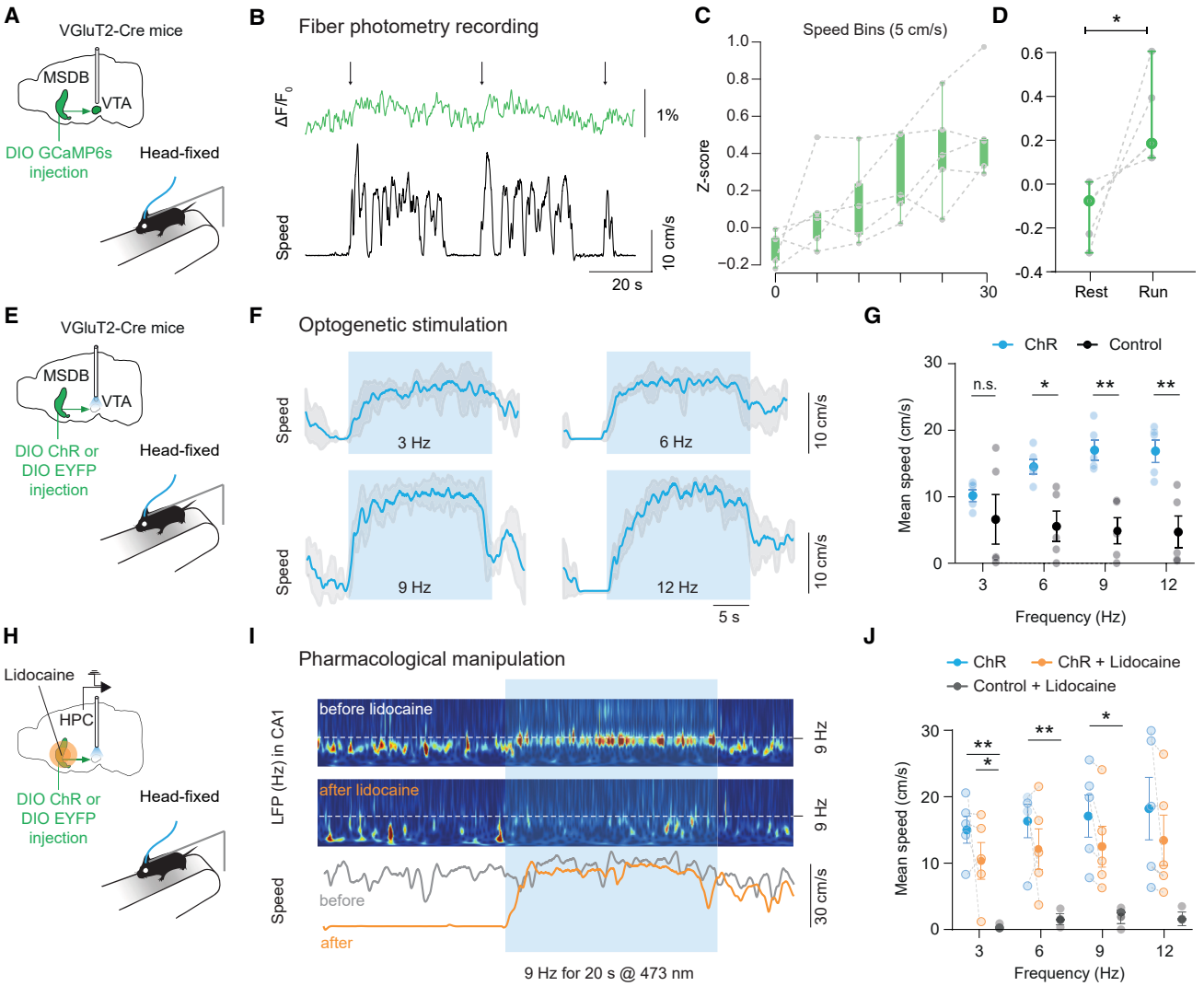

Figure 1. Activity in MSDB$_{glu}$-VTA axons correlates with locomotion and is sufficient to reliably initiate movement when optogenetically stimulated

(A–D) Fiber photometry recordings.

(A) Scheme of injection site, implant, and setup.

(B) Representative example of GCaMP6s fluorescence of MSDB$_{glu}$-VTA axons in different locomotion episodes in a head-fixed mouse on a treadmill. Arrows indicate the time of movement onset. Upper trace: ΔF/F signal recorded in MSDB$_{glu}$-VTA axons. Lower trace: corresponding speed trace.

(C) *Z* score fluorescence correlates with locomotor speed (velocity is binned in 5 cm/s from 0 to 30 cm/s, n = 4 GCaMP6s mice).

(D) Difference in *Z* score between running and resting phases (n = 4 GCaMP6s mice, average across all trials; paired t test).

(E–G) Optogenetic manipulation.

(E) Scheme of injection site and experimental setup.

(F) Representative example of 20 s optogenetic stimulation at different frequencies in the same animal. Five repetitions, mean and SD displayed.

(G) Mean locomotor speed at different stimulation frequencies (n = 5 MSDB$_{glu}$-VTA:ChR mice, n = 5 MSDB$_{glu}$-VTA:EYFP mice; repeated measures (RM) two-way ANOVA: group × frequency interaction, F(3,24) = 9.363, p = 0.0003; Sidak's multiple comparison test).

(H–J) Optogenetic stimulation with pharmacological manipulation.

(H) Scheme of injection site and experimental setup.

(I) Representative spectrogram of CA1 LFP during 9 Hz stimulation of MSDB$_{glu}$-VTA axons. Upper panel: spectrogram before lidocaine injection. Middle panel: spectrogram after lidocaine injection. Lower panel: corresponding speed trace before (gray) and after (orange) lidocaine injection.

(J) Mean locomotor speed before and after lidocaine injection (n = 5 MSDB$_{glu}$-VTA:ChR mice before and after lidocaine injection; n = 3 MSDB$_{glu}$-VTA:Ctrl mice after lidocaine injection; RM two-way ANOVA: group interaction, F(2,10) = 6.903, p = 0.0131; Tukey's multiple comparison test). All data are presented as mean ± SEM. n.s., non-significant, *p < 0.05, **p < 0.01. See also Figures S1–S4.

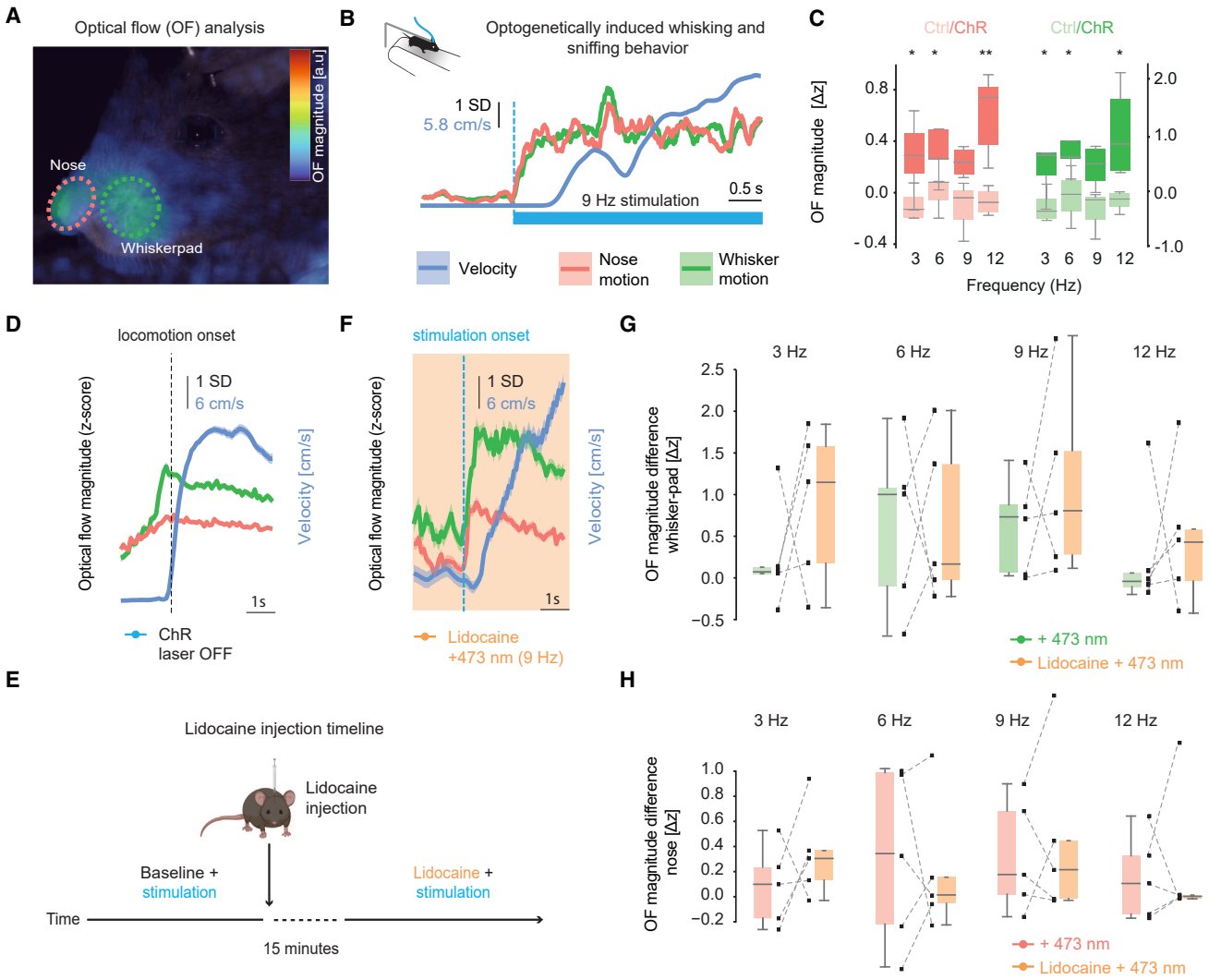

Figure 2. Increase of sniffing and whisking behavior preceding optogenetically evoked locomotion onset

(A) Representative frame from an infrared camera recording superimposed with optical flow analysis. Dotted lines represent automatically detected nose (red) and whisker pad (green) areas.

(B) Representative trace showing sniffing (red) and whisking (green) behavior elicited by optogenetic stimulation (bright blue dashed line) preceding locomotion (blue).

(C) Optical flow magnitude difference (post-stimulation—pre-stimulation) between optogenetically induced sniffing (left panel) and whisking (right panel) in $MSDB_{glu}$-VTA:ChR (bold color) and $MSDB_{glu}$-VTA:EYFP (shaded color) mice at different stimulation frequencies (n = 5 $MSDB_{glu}$-VTA:ChR mice, n = 3 $MSDB_{glu}$-VTA:EYFP mice, average across all trials; one-sample t test against a difference of 0).

(D) *Z* score magnitude of nose (red) and whisker pad (green) movement aligned to the onset (black dashed line) of spontaneous locomotor episodes (blue) in $MSDB_{glu}$-VTA:ChR mice without optogenetic stimulation (n = 5 $MSDB_{glu}$-VTA:ChR mice).

(E) Scheme of lidocaine injection timeline.

(F) *Z* score magnitude of nose (red) and whisker pad (green) movement aligned to the onset (blue dashed line) of 9 Hz optogenetically evoked locomotor episodes (blue) in $MSDB_{glu}$-VTA:ChR mice after lidocaine injection (n = 5 $MSDB_{glu}$-VTA:ChR mice).

(G and H) Optical flow magnitude difference (post-pre stimulation) between optogenetically induced sniffing (G) and whisking (H) before and after lidocaine injection at different stimulation frequencies (n = 5 $MSDB_{glu}$-VTA:ChR mice, average across all trials, pairwise t test with Bonferroni correction). All data are presented as mean ± SEM. *p < 0.05, **p < 0.01. See also Video S1.

$MSDB_{glu}$-VTA circuit promotes environmental exploration

Because VTA circuits can encode for both rewarding and aversive stimuli,[29] we examined whether the increased locomotion and exploratory actions were associated with a specific valence. To do this, we tested $MSDB_{glu}$-VTA:ChR and $MSDB_{glu}$-VTA:EYFP mice in both a novel cue test (Figures 4A–4C) and an open-field anxiety test (Figures 4D–4J). First, we designed a behavioral paradigm in which mice were exposed to a series of novel cues (object, food, or another mouse). To confirm the

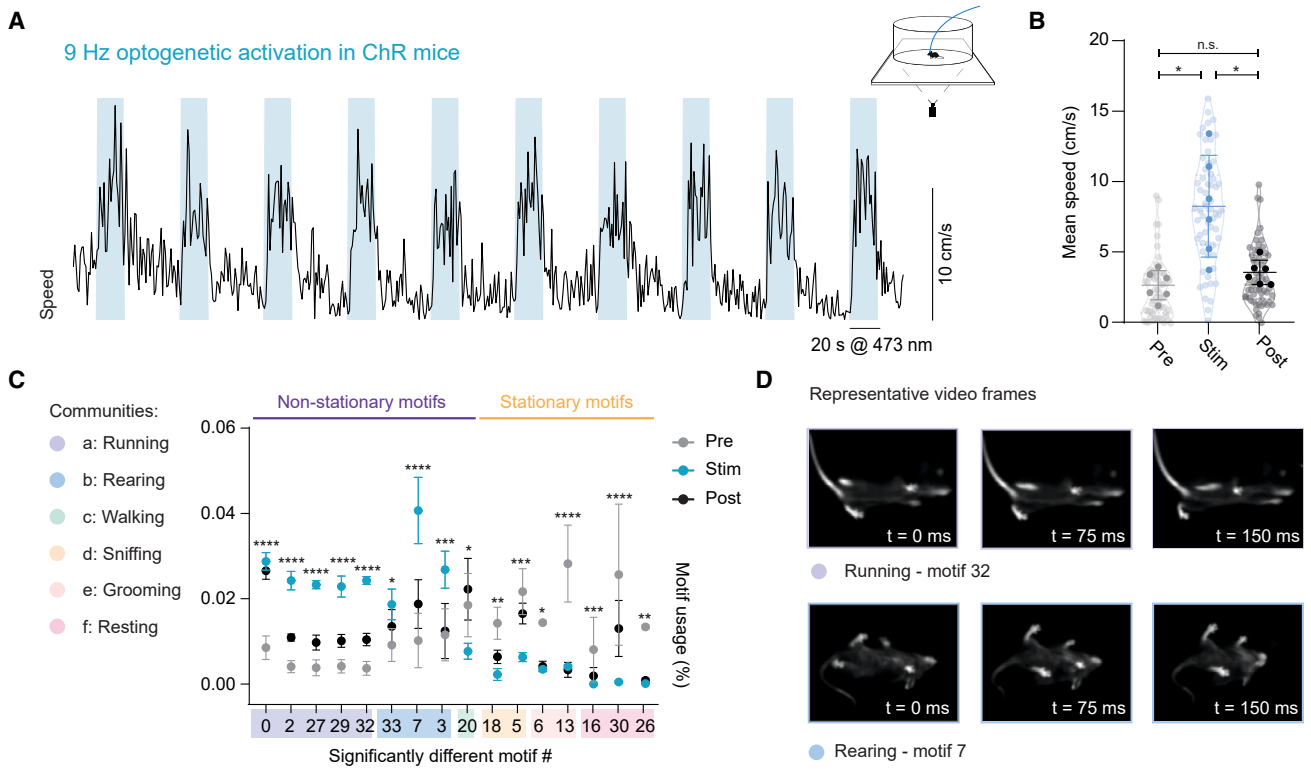

Figure 3. Optogenetic stimulation in freely moving animals increases exploratory actions

(A) Representative example of speed modulation upon optogenetic stimulation in an open-field arena (20 s pre-stimulation epoch, 20 s stimulation epoch, 20 s post-stimulation epoch, 10 repetitions, mean, 9 Hz optogenetic stimulation).

(B) Mean locomotor speed increases with optogenetic stimulation (n = 6 $MSDB_{glu}$-VTA:ChR mice, 10 repetitions per mouse; RM one-way ANOVA, pre-, stim, and post-optogenetic stimulation epochs, F(1.014,5.072) = 12.04, p = 0.0173; Tukey's multiple comparisons *p < 0.05).

(C) Significantly different VAME motif percentage prevalence during pre-, stim, and post-stimulation epochs (n = 3 $MSDB_{glu}$-VTA:ChR mice, RM two-way ANOVA: motifs × pre-stim-post interaction, F(68, 136) = 6.936, p < 0.0001; Sidak's multiple comparison test).

(D) Representative examples of video frames segmented by VAME for the significantly different motif number 32 (running motif) and 7 (rearing motif). See also Figure S5 and Video S2.

locomotor effect of the $MSDB_{glu}$-VTA stimulation, we applied the same activation pattern as previously used in the open-field condition for all three novel cues (Figure S6A). In line with our observations in the open-field arena, we found an increase in locomotor speed and VAME running motifs (Figures S6B and S6C). All animals spent more time approaching the social stimulus compared with a novel object or food (Figure S6D) as previously reported also in other studies.[30,31] Given that our stimulation was not spatially confined in this paradigm, we hypothesized that a surprising reward delivery could evoke the described behavior. Thus, we further tested whether the specific activation of this circuit near the cue would modulate the exploration of the animal toward it (Figure 4A). To additionally reduce the confounding effect of neophobia during exposure to novelty,[32,33] we modified the paradigm by introducing 10 min exploration time without stimulation, followed by 10 min exploration with optogenetic stimulation in proximity to the novel cue. We reasoned that this modification of the paradigm would reveal a potential valence-specific response following $MSDB_{glu}$-VTA manipulation. Quantification of mean speed and time spent approaching the novel cue showed the highest values when the social stimulus was explored compared with food or an object, a finding in line with previous literature[30,31] as well as our results above. When comparing the effect of the spatially confined optogenetic stimulation between $MSDB_{glu}$-VTA:ChR and $MSDB_{glu}$-VTA:EYFP for each novel stimulus, we observed a significant increase in the approach time toward the novel object (Figures 4B and 4C). While the $MSDB_{glu}$-VTA circuit activation did not affect the behavior of the animals toward a homeostatic stimulus, such as food or a conspecific, it did increase the number of approaches toward the object. Collectively, the analysis indicates that this behavior reflects environment-oriented exploration.

Increased locomotion and exploration may also represent a proxy for stress and anxiety.[34,35] Therefore, we tested the animals in an open-field anxiety test. Mice were placed in a previously unexplored arena of 70 cm diameter with 200 lux light intensity in the center and 10 lux intensity on the walls (Figure 4D). In this test, a reduction in both locomotion and frequency of center crossings is typically associated with increased stress or anxiety.[36] First, we confirmed that we could reliably increase the speed of locomotion of $MSDB_{glu}$-VTA:ChR mice during stimulation in this setting (Figure 4E). The increase in movement not only

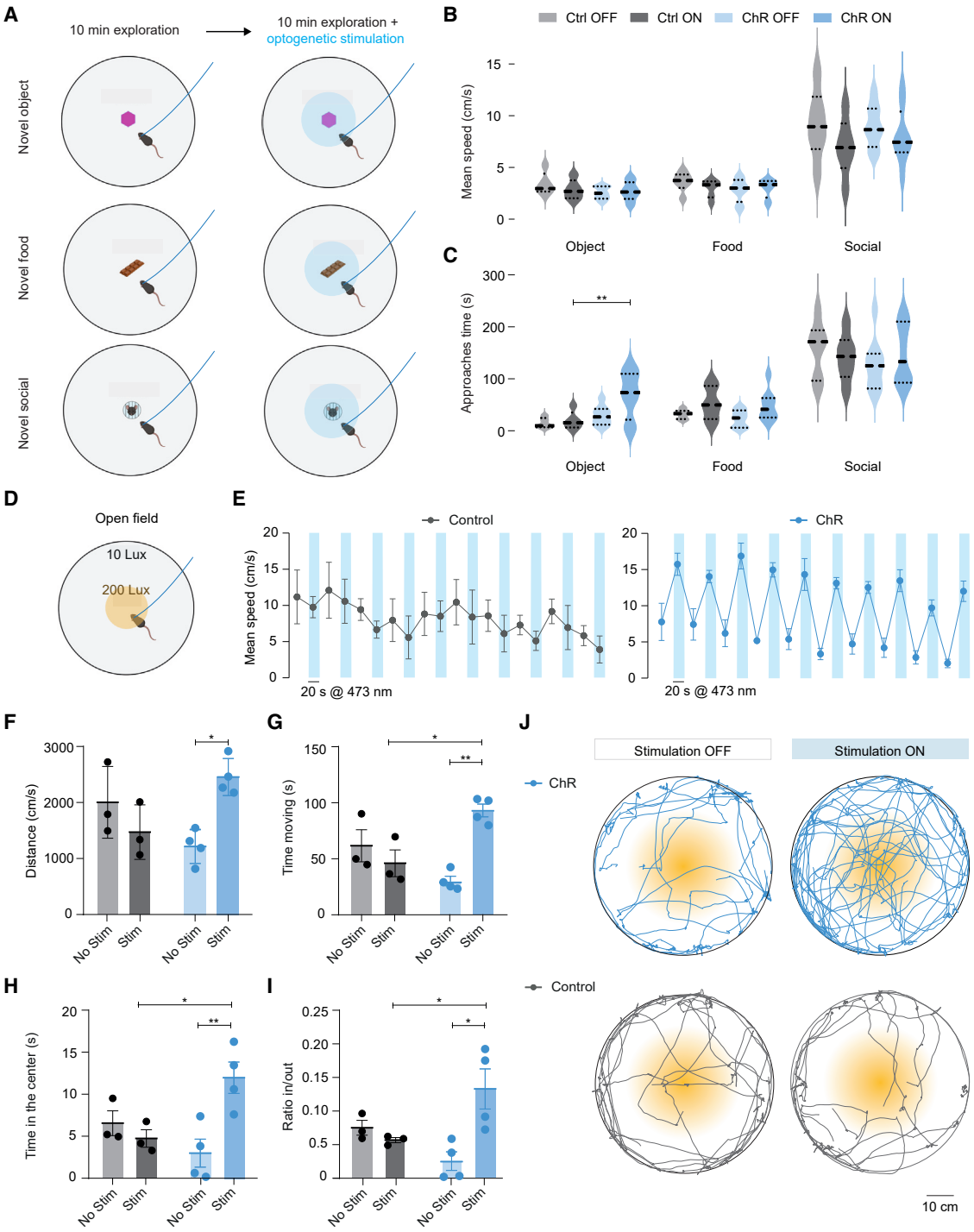

Figure 4. Optogenetic manipulation of the MSDB$_{glu}$-VTA circuit in a value-specific task

(A) Experimental setup of the novel cue paradigm: mice were exposed for 10 min to the novel object, food, or another mouse. In the next 10 min, they received a spatially confined optogenetic stimulation close to the novel cue.

(B) Mean speed during the spatially confined optogenetic stimulation (three-way ANOVA: novel cue × optogenetic stimulation × group interaction, $F(2,35) = 0.2596$, $p = 0.7728$).

(C) Time spent approaching the novel cues during the spatially confined optogenetic stimulation (three-way ANOVA: novel cue × optogenetic stimulation × group interaction, $F(2,35) = 0.7988$, $p = 0.4579$; RM two-way ANOVA: stimulation × condition interaction in novel object: $F(1,11) = 6.605$, $p = 0.0260$; Tukey's multiple comparison test) (for the novel cue tests n = 8 MSDB$_{glu}$-VTA:ChR mice, n = 6 MSDB$_{glu}$-VTA:EYFP mice;).

(D) Experimental setup of the open-field anxiety test.

(legend continued on next page)

resulted in higher speeds, larger total distances, and longer time spent moving but also led to an increased time spent in the center of the arena for $MSDB_{glu}$-VTA:ChR mice compared with $MSDB_{glu}$-VTA:EYFP controls (Figures 4F–4J). This suggests that optogenetic stimulation of the $MSDB_{glu}$-VTA pathway was instrumental to overcome the innate anxiety arising in the open field while increasing environmental exploration.

$MSDB_{glu}$-VTA network inhibition reduces locomotion and exploration

After investigating the effects of optogenetic circuit activation, we tested the behavioral output following $MSDB_{glu}$-VTA circuit inhibition during freely moving behavior (Figure 5A). We injected VGluT2::Cre mice with either an inhibitory opsin (AAV9-FLEX-Arch-GFP) ($MSDB_{glu}$-VTA:Arch) or an appropriate control construct (AAV9-EF1a-DIO-EYFP) ($MSDB_{glu}$-VTA:EYFP). *In vitro* patch-clamp (Figures S7A–S7D) and multi-electrode array (Figures S7E–S7J) recordings confirmed the efficient hyperpolarization of $MSDB_{glu}$ $Arch^+$ neurons and the reduced firing frequency of postsynaptic neurons receiving inputs from $MSDB_{glu}$ $Arch^+$ axons. When inhibiting the $MSDB_{glu}$-VTA pathway, we observed a reliable reduction of the mean speed, the distance traveled, and the time spent moving in $MSDB_{glu}$-VTA:Arch mice, while the control group did not display any significant difference (Figures 5B–5D). Thus, manipulating the $MSDB_{glu}$-VTA pathway exerts bidirectional control over the animal's locomotor activity.

To further investigate the optogenetically induced exploratory drive, we tested mice in the elevated plus maze (EPM) test. The EPM creates an approach-avoidance conflict: the novelty of the maze drives innate exploration (approach), while the open, elevated arms have been shown to induce fear and discomfort (avoidance).[37] Entering the open arms allows animals to collect spatial information, and head-dipping behavior has been reported as a form of exploration in this specific test.[38] We optogenetically activated or inhibited the $MSDB_{glu}$-VTA network while animals were in the EPM closed arms (Figures 5E and 5F), which can be considered safe zones for the mice. If the activation of the circuit was inducing a purely locomotor behavior, one might expect increased running activity confined to these closed arms. However, the $MSDB_{glu}$-VTA:ChR mice displayed increased exploratory behavior, as shown by an increased amount of time spent in the open arms, a higher number of open arm entries, and more prominent head-dipping behavior. Conversely, $MSDB_{glu}$-VTA:Arch mice spent less time in the open arms and displayed less head-dipping behavior, similar to control mice (Figures 5G–5J). Interestingly, the analysis of the population variance revealed that $MSDB_{glu}$-VTA:Arch mice had a smaller standard deviation than control mice in the time spent in the open and closed arm and in the percentage of head dipping, which suggests that this significant reduction in behavioral variability is a result of circuit inhibition. Taken together, these results indicate that the $MSDB_{glu}$-VTA circuit contributes to solving the animal's approach-avoidance conflict by promoting exploratory behavior and reducing innate fear of novel environments.

$MSDB_{glu}$ inputs monosynaptically target a heterogeneous VTA cell population

Following the identification of this glutamatergic basal forebrain to midbrain pathway, we next aimed to determine the cellular connectivity. First, we performed immunostainings for the presynaptic marker protein synapsin I in VGluT2::Cre mice expressing AAV1-EF1a-DIO-EYFP in the MSDB and AAV1-FLEX-tdTomato in the VTA. As expected, we found $MSDB_{glu}$ synapsin I axon terminals in the proximity of identified tyrosine hydroxylase (TH) and tdTomato-positive neurons, as well as neurons co-labeled with both TH and tdTomato in the VTA (Figures S8A–S8D). Moreover, we confirmed the existence of a $MSDB_{glu}$ to VTA_{glu} synaptic contacts as demonstrated by the proximity of the presynaptic protein Bassoon in $MSDB_{glu}$ axons and the postsynaptic protein Shank3 in VTA_{glu} neurons (Figure S8E). To validate the functional relevance of our anatomical findings, we performed whole-cell patch-clamp recordings of VTA neurons in acute slices of VGluT2::Cre mice that were injected with AAV2/1-DIO-ChR-EYFP in MSDB (Figure 6A). We recorded the electrophysiological properties of the patched neurons and photoactivated $MSDB_{glu}$ axonal terminals to elicit excitatory postsynaptic potentials (EPSPs) in targeted cells. We found that 68% of the patched VTA neurons exhibited EPSPs, of which 43% responded with subthreshold and 25% with suprathreshold activity (Figures 6B and 6C). These results indicate that the number of synaptic terminals of the $MSDB_{glu}$-VTA projections is sufficiently high to depolarize and drive spiking in a substantial population of target neurons. In addition, we quantified the $MSDB_{glu}$-VTA monosynaptic connectivity. Bath application of 2,3-dioxo-6-nitro-7-sulfamoyl-benzo[f]quinoxaline (NBQX) and D-(-)-2-Amino-5-phosphonopentanoic acid (D-AP5), as well as tetrodotoxin (TTX) and 4-amynopyridine (4-AP) confirmed the glutamatergic and monosynaptic nature of these projections (Figure 6D). Overall, ∼15% of the patched neurons received monosynaptic glutamatergic inputs from MSDB (n = 16 connected neurons out of 106 patched cells; Figure 6E), consistent with the small and sparse MSDB projections to the VTA reported in previous studies.[12,39,40] VTA neurons responding to $MSDB_{glu}$ inputs were found throughout the anterior-posterior and medio-lateral axess of the VTA region, suggesting target heterogeneity (Figure 6F). To further characterize this heterogeneity, we

(E) Mean locomotor speed in $MSDB_{glu}$-VTA:ChR and $MSDB_{glu}$-VTA:EYFP mice during stimulation and non-stimulation periods.
(F) Distance traveled (group × stimulation interaction, $F(1,5) = 46.95$, $p = 0.0010$).
(G) Time spent moving (group × stimulation interaction, $F(1,5) = 211.2$, $p < 0.001$).
(H) Time spent in the center (group × stimulation interaction, $F(1,5) = 10.71$, $p = 0.0221$).
(I) Ratio of the time spent in the center and the time spent in the periphery of the arena (group × stimulation interaction, $F(1,5) = 10.71$, $p = 0.0221$).
(J) Open-field arena occupancy of one exemplary $MSDB_{glu}$-VTA:ChR and one $MSDB_{glu}$-VTA:EYFP mouse with and without optogenetic stimulation (for the anxiety test n = 4 $MSDB_{glu}$-VTA:ChR mice, n = 3 $MSDB_{glu}$-VTA:EYFP mice; two-way ANOVA with Tukey's multiple comparison test). All data are presented as mean ± SEM. *$p < 0.05$, **$p < 0.01$, ****$p < 0.0001$. See also Figure S6.

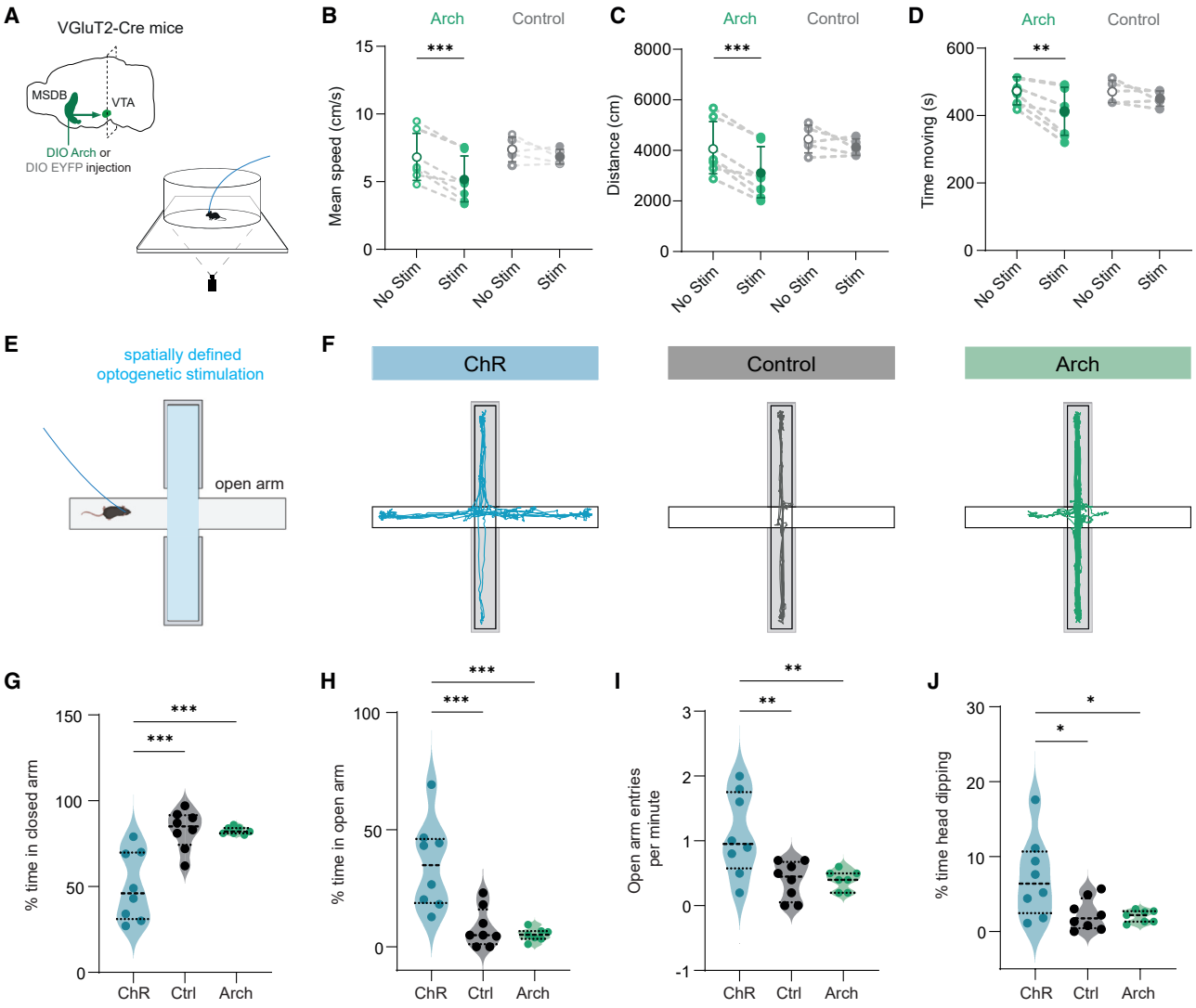

Figure 5. Optogenetic inhibition in freely moving animals decreases locomotion

(A) Scheme of injection site and experimental setup.

(B) Mean locomotor speed in cm/s (RM two-way ANOVA: stimulation × group interaction, $F(1,10) = 7.239$, $p = 0.0227$).

(C) Distance traveled in cm (RM two-way ANOVA: stimulation × group interaction, $F(1,10) = 7.239$, $p = 0.0227$).

(D) Time moving in s (RM two-way ANOVA: stimulation × group interaction, $F(1,10) = 3.616$, $p = 0.0864$). (B–D: n = 7 $MSDB_{glu}$-VTA:Arch mice, n = 5 $MSDB_{glu}$-VTA:EYFP mice; Sidak's multiple comparison test).

(E) Experimental setup in the EPM test.

(F) Representative traces of $MSDB_{glu}$-VTA:ChR, $MSDB_{glu}$-VTA:EYFP, and $MSDB_{glu}$-VTA:Arch injected mice in the EPM.

(G) Time spent in the closed arm (one-way ANOVA, $F(2,20) = 14.77$, $p = 0.0001$; Arch vs. Ctrl unpaired t test, $F(7,6) = 38.08$, $p = 0.0007$).

(H) Time spent in the open arm (one-way ANOVA, $F(2,20) = 13.85$, $p = 0.0002$, Arch vs. Ctrl unpaired t test, $F(7,6) = 9.551$, $p = 0.0138$).

(I) Number of open arm entries per minute (one-way ANOVA, $F(2,20) = 7.262$, $p = 0.0043$).

(J) Time head dipping in the open arm (one-way ANOVA, $F(2,20) = 5.682$, $p = 0.0111$; Arch vs. Ctrl unpaired t test, $F(7,6) = 6.587$, $p = 0.0352$). (E–J: n = 8 $MSDB_{glu}$-VTA:ChR mice, n = 8 $MSDB_{glu}$-VTA:EYFP mice, n = 7 $MSDB_{glu}$-VTA:Arch mice; Tukey's multiple comparison test). All data are presented as mean ± SEM. *$p < 0.05$, **$p < 0.01$, ***$p < 0.001$. See also Figure S7.

used immunohistological staining for TH and a viral injection of AAV1-FLEX-tdTomato in the VTA of n = 5 VGluT2::Cre mice to identify dopaminergic (DA), glutamatergic, and double-labeled cells receiving monosynaptic $MSDB_{glu}$ inputs (Figures 6G and 6H). In addition, we performed hierarchical cluster analysis over the electrophysiological features of VTA recorded neurons (n = 145, Figure S9). Five clusters emerged (Figure S9A), and monosynaptically targeted VTA neurons were found in all clusters (Figure S9B). In line with previous literature,[41,42] the electrophysiological features of these cells were not predictive of their immunohistochemical identity, and we found $VGluT2^+$ neurons in all clusters and TH^+ neurons in four out of the five clusters

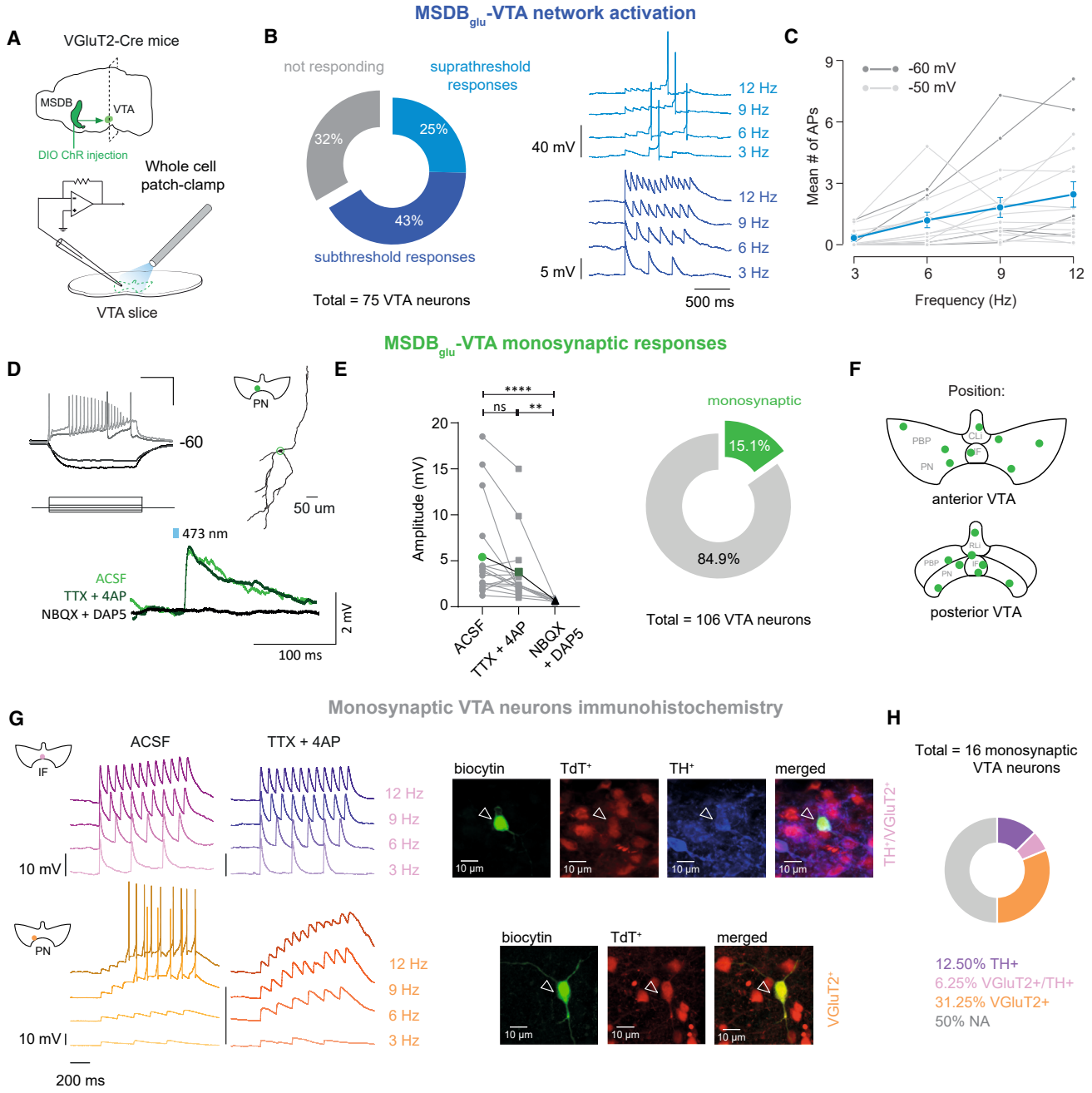

Figure 6. Electrophysiological features of MSDB$_{glu}$ targeted VTA neurons

(A) Scheme of injection site and experimental setup.

(B) Left panel: percentage of VTA neurons responding upon optogenetic stimulation (light blue: suprathreshold responses; dark blue: subthreshold responses; gray: not responding). Right panel: exemplary traces of a suprathreshold and subthreshold response in patched VTA neurons at different stimulation frequencies.

(C) Mean number of APs elicited by optogenetic stimulation in suprathreshold responding neurons (n = 19 VTA neurons, mean in blue). Cells were recorded at a holding membrane potential of either −50 mV (light gray) or −60 mV (dark gray).

(D) Representative example of whole-cell-recorded VTA neuron. Upper left: response to 500 ms current injections (scale bar: 100 ms, 20 mV/200 pA). Upper right: cell position in VTA and cell morphology after reconstruction. Bottom panel: EPSP in response to light stimulation of ChR$^+$ MSDB$_{glu}$ neurons. Light green: ACSF/control condition. Dark green: bath application of TTX and 4-AP. Black: bath application of NBQX and DAP5.

(E) Left panel: EPSP amplitude quantification (n = 16 cells, in gray single-cell values, in bold colors mean values, Kruskal-Wallis test, $p < 0.0001$; Dunn's multiple comparison test $^{**}p < 0.001$, $^{****}p < 0.0001$). Right panel: percentage of VTA neurons receiving monosynaptic MSDB$_{glu}$ inputs.

(F) Localization of VTA neurons receiving monosynaptic MSDB$_{glu}$ inputs.

(G) Exemplary responses of two VTA neurons receiving monosynaptic inputs from MSDB$_{glu}$ axons. Left panel: localization of the cell in the VTA and optogenetic response at different stimulation frequencies in ACSF and TTX-4-AP condition. Right panels: immunohistochemistry of the two exemplary cells.

(H) Percentage of TH$^+$, VGluT2$^+$, and co-labeled cells recovered from the monosynaptic VTA neurons. See also Figures S8 and S9.

(Figures S9C and S9D). When comparing each cluster feature based on well-known electrophysiological parameters such as rheobase, input resistance, sag index, rebound index, and action potential latency, we found clear differences between the groups (Figures S9E–S9G). The highest number of monosynaptically connected neurons was observed in cluster 1 and located in the medial VTA, in line with our axonal density quantification (Figure S2C). This cluster was characterized by neurons showing high rheobase, high input resistance, and high latency before the first action potential firing, resembling the properties of the glutamate-GABA (gamma-aminobutyric acid) co-releasing neurons recently described in VTA.[43] Overall, these data demonstrate the existence of a monosynaptic glutamatergic MSDB projection targeting a molecularly and functionally heterogeneous population of VTA neurons capable of driving a strong circuit response in the VTA.

DISCUSSION

In this study, we reveal that the activity of $MSDB_{glu}$ axons in VTA bidirectionally drives locomotion and exploration. Exploratory behaviors result from various kinds of motivations that can be broadly categorized into homeostatic needs and environmental curiosity.[4,33,44,45] The pursuit of homeostatic needs leads to goal-seeking behavior: animals perform a series of operant tasks and conditioned responses to obtain food or water. In this paradigm, the exploratory behavior is interrupted in the moment the animal reaches its goal. By contrast, environmental curiosity is not dependent on any immediate external goal or reward. It results from the animal's internal drive to explore a given environment and is expressed as a set of behavioral responses including walking, rearing, whisking, and sniffing.[2] To identify and quantify such behaviors in the absence of reinforcing stimuli, we leveraged machine learning tools in both head-fixed and freely moving mice. It has been shown that rodents move their nose and vibrissae to explore their peri-personal space,[46] while sniffing has been associated with motivated behavior.[47] Under head-fixed conditions, we observed the same orofacial movements preceding optogenetically induced locomotion, thus indicating an increase of exploratory and motivated actions upon activation of the circuit. Interestingly, it has also been observed that during bouts of exploration, whisking and sniffing are phase-locked within the theta-frequency range[48] that is in turn regulated by the septo-hippocampal network.

We previously showed that the stimulation of $MSDB_{glu}$ neurons elicits locomotion and hippocampal theta generation prior to locomotion onset[7]; here, we demonstrate that locomotion can be reliably initiated via activation of projections to VTA and that those specific inputs are increasing exploratory-like behavior prior to its onset. As head-fixed animals are relatively limited in their behavioral repertoire, we activated the $MSDB_{glu}$-VTA pathway in a series of experiments where mice can move freely. In the open field, we detected an increase in rearing, which is considered a way for the animal to sample environmental information, especially when cues are distant and otherwise inaccessible. To disentangle if this exploratory behavior is oriented toward the environment or toward cues of specific valence, we exposed the mice to a novel object, food, or another mouse. We reasoned that the spatially confined optogenetic activation of the pathway in the presence of novel cues may reveal specificity in the exploratory drive. As reported in previous studies,[30,31] we found that both control and opsin mice spent more time investigating the novel mouse rather than the novel object or food. However, when comparing the approach time during optogenetic stimulation, we saw an increased time approaching the object in opsin mice compared with controls. This suggests that while the activation of the $MSDB_{glu}$-VTA pathway does not modulate the innate exploratory drive toward homeostatic cues such as food or conspecifics, it does increase the interest toward environmental cues such as a novel object.

Rearing and environmental exploration could also represent a proxy of escaping behavior, with the mice exploring the environment to find a shelter or an exit point.[33,35] For this reason, we performed an anxiety test where the animals were exposed to a novel and potentially dangerous environment. This situation is expected to drive thigmotaxis, freezing, and jumping behavior.[2] Instead, stimulation of the $MSDB_{glu}$-VTA circuit increased not only locomotion during the anxiety test but also the time spent in the center of an open field and in the open arms of an EPM, further supporting the increased exploratory behavior evoked by the upregulation of this pathway. By contrast, inhibiting the $MSDB_{glu}$-VTA pathway in the open-field arena led to a significant reduction in locomotor speed and distance traveled, as well as reduced time spent moving and exploratory drive in the EPM. Taken together, these results reveal that the $MSDB_{glu}$-VTA circuit bidirectionally modulates locomotion and exploratory behavior. Sniffing and whisking allow the animal to sample a higher number of peri-personal information, while rearing gives access to distant environmental cues, independently of the nature of the stimulus that is presented. Our data are in line with previous studies suggesting a role of this network in motivation and information-seeking behavior.[49] Indeed, mice increase lever pressing for intracranial self-stimulation of the $MSDB_{glu}$-VTA axons in the absence of any reward, and this activation increases DA release in the nucleus accumbens.[49] This study corroborates the role of the $MSDB_{glu}$-VTA network in information-seeking behavior and shows that theta-frequency stimulation of this circuit increases an animal's drive to explore the environment and promotes approach when the animal faces an approach-avoidance conflict.

These findings also raise the question of which VTA subpopulations may receive $MSDB_{glu}$ inputs. Anatomical data revealed that only 2% of the total glutamatergic projections reaching VTA arise from the MSDB,[12] and tracing data that labeled the entire septal region reported projections targeting DAT^+, GAD^+, and $VGluT2^+$ neurons in the VTA.[39] Here, we provide circuit mapping results showing that optogenetic activation of $MSDB_{glu}$ axons reliably induced EPSPs in VTA neurons even in the presence of action potential blockers, functionally demonstrating the monosynaptic nature of this projection. VTA-responding neurons included glutamatergic ($VGluT2^+$), putative dopaminergic (TH^+), and putative co-releasing cells ($TH^+/VGluT2^+$) in agreement with previous studies that reported a high variability of VTA cell types with regard to their electrophysiological properties as well as neurotransmitter release and co-release.[42,50,51] How can the $MSDB_{glu}$ inputs targeting a heterogeneous VTA

circuit give rise to a distinct behavioral outcome? It was shown that multiple brain regions send qualitatively similar yet quantitatively different inputs to the three distinct cell populations within the VTA.[52] Thus, it stands to reason that depending on the animal's internal state and external environment, the strength of these inputs changes. Key circuits involved in motivation, homeostasis, and fear responses project to the VTA and innervate all cell types. We hypothesize that the behavioral outcome is computed within the diverse VTA network to produce a coherent and unified behavioral response based on the relative strength that different inputs generate at each time point.

In conclusion, we have identified a subcortical glutamatergic circuit that bidirectionally mediates locomotion and exploration. This places the MSDB at the critical interface of the spatial and cognitive map formation via septo-hippocampal projections and the execution of information-seeking behavior via VTA projections.

STAR★METHODS

Detailed methods are provided in the online version of this paper and include the following:

- KEY RESOURCES TABLE
- RESOURCE AVAILABILITY
  - Lead contact
  - Materials availability
  - Data and code availability
- EXPERIMENTAL MODEL AND STUDY PARTICIPANT DETAILS
- METHOD DETAILS
  - Stereotactic viral injection
  - Chronic surgery
  - Behavioral tests
  - Head-fixed experiments
  - Head-fixed reward learning task
  - Open field
  - Open field anxiety test
  - Elevated plus maze (EPM) test
  - Fiber photometry recordings
  - Optogenetic recordings
  - Pharmacological manipulation
  - LFP recordings
  - Electrophysiological recordings in brain slices
  - Multielectrode array (MEA) recordings
  - Antibody staining
- QUANTIFICATION AND STATISTICAL ANALYSIS
  - Data analysis
  - Statistical analysis

SUPPLEMENTAL INFORMATION

Supplemental information can be found online at https://doi.org/10.1016/j.neuron.2023.12.016.

ACKNOWLEDGMENTS

We thank Liset Menendez de la Prida and Viktor Varga for the comments on this manuscript; Jürgen Goldschmidt, Oliver Kobler, and the whole Leibniz Institute for Neurobiology (LIN) Combinatorial NeuroImaging Core Facility for the help with image acquisition; Janina Juhle and Peter Kolch for the technical support; and the entire S.R. laboratory for insightful discussions. The resources for all experiments were provided by the German Center for Neurodegenerative Diseases (DZNE) and LIN. Elements in the graphical abstract and Figures 2E, 4A, 4D 5E, and S6A were created with BioRender.com. The authors received funding from the German Research Foundation (DFG) CRC 1436 - project 425899996 (A03 to S.R., A02 and Z01 to M.R.K., B06 to J.M.P.P.), CRC 1089 (to S.R.), RTG 2413 SynAGE project 362321501 (to S.R., J.M.P.P., and M.R.K.), and FOR5228 (RP06 to A.K. and M.R.K.); Leibniz SAW Learning Resilience (to S.R.); and ERC Consolidator grant Sub-D-Code (to S.R.). A.K. was supported by the Leibniz Institute for Neurobiology (LIN) special project. S.M. was supported by the Swedish Research Council (project 2017-06254), Leibniz Best Minds StartUp grant (J143/2022), and German Center for Mental Health (DZPG, project 01EE2305E).

AUTHOR CONTRIBUTIONS

Conceptualization, P.M., S.M., and S.R.; software, K.L., O.B., D.D., and H.K.; formal analysis, P.M., O.B., K.L., H.K., and S.M.; investigation, P.M., H.K., S.V., A.K., and J.U.H.; resources, F.F., J.M.P.P., and M.R.K.; visualization, P.M., O.B., A.K., and H.K.; writing – original draft, P.M. with help from O.B., S.M., and S.R.; writing – review & editing, P.M., O.B., A.K., J.M.P.P., M.R.K., S.M., and S.R.; supervision, S.M. and S.R.; funding acquisition, S.R.

DECLARATION OF INTERESTS

The authors declare no competing interests.

Received: September 15, 2022
Revised: November 10, 2023
Accepted: December 20, 2023
Published: January 23, 2024

REFERENCES

1. Mogenson, G.J., Jones, D.L., and Yim, C.Y. (1980). From motivation to action: Functional interface between the limbic system and the motor system. Prog. Neurobiol. *14*, 69–97.
2. Belzung, C. (1999). Measuring rodent exploratory behavior. In Techniques in the Behavioral and Neural Sciences (Elsevier), pp. 738–749.
3. Renner, M.J., and Seltzer, C.P. (1991). Molar characteristics of exploratory and investigatory behavior in the rat (Rattus norvegicus). J. Comp. Psychol. *105*, 326–339.
4. Kesner, A.J., Calva, C.B., and Ikemoto, S. (2022). Seeking motivation and reward: Roles of dopamine, hippocampus, and supramammillo-septal pathway. Prog. Neurobiol. *212*, 102252.
5. Brandon, M.P., Bogaard, A.R., Libby, C.P., Connerney, M.A., Gupta, K., and Hasselmo, M.E. (2011). Reduction of Theta Rhythm Dissociates Grid Cell Spatial Periodicity from Directional Tuning. Science *332*, 595–599.
6. Cazala, P., Galey, D., and Durkin, T. (1988). Electrical self-stimulation in the medial and lateral septum as compared to the lateral hypothalamus: Differential intervention of reward and learning processes? Physiol. Behav. *44*, 53–59.
7. Fuhrmann, F., Justus, D., Sosulina, L., Kaneko, H., Beutel, T., Friedrichs, D., Schoch, S., Schwarz, M.K., Fuhrmann, M., and Remy, S. (2015). Locomotion, Theta Oscillations, and the Speed-Correlated Firing of Hippocampal Neurons Are Controlled by a Medial Septal Glutamatergic Circuit. Neuron *86*, 1253–1264.
8. Koenig, J., Linder, A.N., Leutgeb, J.K., and Leutgeb, S. (2011). The Spatial Periodicity of Grid Cells Is Not Sustained During Reduced Theta Oscillations. Science *332*, 592–595.
9. Zhang, G.W., Shen, L., Zhong, W., Xiong, Y., Zhang, L.I., and Tao, H.W. (2018). Transforming Sensory Cues into Aversive Emotion via Septal-Habenular Pathway. Neuron *99*, 1016–1028.e5.

10. Zhang, G.W., Sun, W.J., Zingg, B., Shen, L., He, J., Xiong, Y., Tao, H.W., and Zhang, L.I. (2018). A Non-canonical Reticular-Limbic Central Auditory Pathway via Medial Septum Contributes to Fear Conditioning. Neuron *97*, 406–417.e4.

11. Justus, D., Dalügge, D., Bothe, S., Fuhrmann, F., Hannes, C., Kaneko, H., Friedrichs, D., Sosulina, L., Schwarz, I., Elliott, D.A., et al. (2017). Glutamatergic synaptic integration of locomotion speed via septoentorhinal projections. Nat. Neurosci. *20*, 16–19.

12. Geisler, S., Derst, C., Veh, R.W., and Zahm, D.S. (2007). Glutamatergic Afferents of the Ventral Tegmental Area in the Rat. J. Neurosci. *27*, 5730–5743.

13. Engelhard, B., Finkelstein, J., Cox, J., Fleming, W., Jang, H.J., Ornelas, S., Koay, S.A., Thiberge, S.Y., Daw, N.D., Tank, D.W., et al. (2019). Specialized coding of sensory, motor and cognitive variables in VTA dopamine neurons. Nature *570*, 509–513.

14. Kremer, Y., Flakowski, J., Rohner, C., and Lüscher, C. (2020). Context-Dependent Multiplexing by Individual VTA Dopamine Neurons. J. Neurosci. *40*, 7489–7509.

15. Howe, M.W., and Dombeck, D.A. (2016). Rapid signalling in distinct dopaminergic axons during locomotion and reward. Nature *535*, 505–510.

16. Horvitz, J.C. (2000). Mesolimbocortical and nigrostriatal dopamine responses to salient non-reward events. Neuroscience *96*, 651–656.

17. Morrens, J., Aydin, Ç., Janse van Rensburg, A., Esquivelzeta Rabell, J., and Haesler, S. (2020). Cue-Evoked Dopamine Promotes Conditioned Responding during Learning. Neuron *106*, 142–153.e7.

18. Cador, M., Marco, N., Stinus, L., and Simonnet, G. (2002). Interaction between neuropeptide FF and opioids in the ventral tegmental area in the behavioral response to novelty. Neuroscience *110*, 309–318.

19. Fink, J.S., and Smith, G.P. (1979). Decreased locomotor and investigatory exploration after denervation of catecholamine terminal fields in the forebrain of rats. J. Comp. Physiol. Psychol. *93*, 34–65.

20. Hooks, M.S., and Kalivas, P.W. (1995). The role of mesoaccumbens-pallidal circuitry in novelty-induced behavioral activation. Neuroscience *64*, 587–597.

21. Stuart, G., Spruston, N., Sakmann, B., and Häusser, M. (1997). Action potential initiation and backpropagation in neurons of the mammalian CNS. Trends Neurosci. *20*, 125–131.

22. Waters, J., Schaefer, A., and Sakmann, B. (2005). Backpropagating action potentials in neurones: measurement, mechanisms and potential functions. Prog. Biophys. Mol. Biol. *87*, 145–170.

23. Schultz, W., Dayan, P., and Montague, P.R. (1997). A Neural Substrate of Prediction and Reward. Science *275*, 1593–1599.

24. Grace, A.A., Floresco, S.B., Goto, Y., and Lodge, D.J. (2007). Regulation of firing of dopaminergic neurons and control of goal-directed behaviors. Trends Neurosci. *30*, 220–227.

25. Deschênes, M., Moore, J., and Kleinfeld, D. (2012). Sniffing and whisking in rodents. Curr. Opin. Neurobiol. *22*, 243–250.

26. Mathis, A., Mamidanna, P., Cury, K.M., Abe, T., Murthy, V.N., Mathis, M.W., and Bethge, M. (2018). DeepLabCut: markerless pose estimation of user-defined body parts with deep learning. Nat. Neurosci. *21*, 1281–1289.

27. Barnstedt, O., Mocellin, P., and Remy, S. (2023). A hippocampus-accumbens code guides goal-directed appetitive behavior. Preprint at bioRxiv. https://doi.org/10.1101/2023.03.09.531869.

28. Luxem, K., Mocellin, P., Fuhrmann, F., Kürsch, J., Miller, S.R., Palop, J.J., Remy, S., and Bauer, P. (2022). Identifying behavioral structure from deep variational embeddings of animal motion. Commun. Biol. *5*, 1267.

29. Lammel, S., Lim, B.K., Ran, C., Huang, K.W., Betley, M.J., Tye, K.M., Deisseroth, K., and Malenka, R.C. (2012). Input-specific control of reward and aversion in the ventral tegmental area. Nature *491*, 212–217.

30. Kim, D.G., Gonzales, E.L., Kim, S., Kim, Y., Adil, K.J., Jeon, S.J., Cho, K.S., Kwon, K.J., and Shin, C.Y. (2019). Social Interaction Test in Home Cage as a Novel and Ethological Measure of Social Behavior in Mice. Exp. Neurobiol. *28*, 247–260.

31. Reppucci, C.J., and Veenema, A.H. (2020). The social versus food preference test: A behavioral paradigm for studying competing motivated behaviors in rodents. MethodsX *7*, 101119.

32. Crane, A.L., and Ferrari, M.C.O. (2017). Patterns of predator neophobia: a meta-analytic review. Proc. Biol. Sci. *284*, 20170583.

33. Hughes, R.N. (2007). Neotic preferences in laboratory rodents: issues, assessment and substrates. Neurosci. Biobehav. Rev. *31*, 441–464.

34. Hughes, R.N., Bakhurin, K.I., Petter, E.A., Watson, G.D.R., Kim, N., Friedman, A.D., and Yin, H.H. (2020). Ventral Tegmental Dopamine Neurons Control the Impulse Vector during Motivated Behavior. Curr. Biol. *30*, 2681–2694.e5.

35. Sturman, O., Germain, P.L., and Bohacek, J. (2018). Exploratory rearing: a context- and stress-sensitive behavior recorded in the open-field test. Stress *21*, 443–452.

36. Simon, P., Dupuis, R., and Costentin, J. (1994). Thigmotaxis as an index of anxiety in mice. Influence of dopaminergic transmissions. Behav. Brain Res. *61*, 59–64.

37. Montgomery, K.C. (1955). The relation between fear induced by novel stimulation and exploratory behavior. J. Comp. Physiol. Psychol. *48*, 254–260.

38. Arabo, A., Potier, C., Ollivier, G., Lorivel, T., and Roy, V. (2014). Temporal analysis of free exploration of an elevated plus-maze in mice. J. Exp. Psychol. Anim. Learn. Cogn. *40*, 457–466.

39. Beier, K.T., Gao, X.J., Xie, S., DeLoach, K.E., Malenka, R.C., and Luo, L. (2019). Topological Organization of Ventral Tegmental Area Connectivity Revealed by Viral-Genetic Dissection of Input-Output Relations. Cell Rep. *26*, 159–167.e6.

40. Geisler, S., and Wise, R.A. (2008). Functional Implications of Glutamatergic Projections to the Ventral Tegmental Area. Rev. Neurosci. *19*, 227–244.

41. Margolis, E.B., Coker, A.R., Driscoll, J.R., Lemaître, A.I., and Fields, H.L. (2010). Reliability in the Identification of Midbrain Dopamine Neurons. PLoS One *5*, e15222.

42. Morales, M., and Margolis, E.B. (2017). Ventral tegmental area: cellular heterogeneity, connectivity and behaviour. Nat. Rev. Neurosci. *18*, 73–85.

43. Miranda-Barrientos, J., Chambers, I., Mongia, S., Liu, B., Wang, H.L., Mateo-Semidey, G.E., Margolis, E.B., Zhang, S., and Morales, M. (2021). Ventral tegmental area GABA, glutamate, and glutamate-GABA neurons are heterogeneous in their electrophysiological and pharmacological properties. Eur. J. Neurosci. *54*, 4061–4084.

44. Berlyne, D.E. (1966). Curiosity and exploration. Science *153*, 25–33.

45. Gordon, G., Fonio, E., and Ahissar, E. (2014). Emergent Exploration via Novelty Management. J. Neurosci. *34*, 12646–12661.

46. Kurnikova, A., Moore, J.D., Liao, S.M., Deschênes, M., and Kleinfeld, D. (2017). Coordination of Orofacial Motor Actions into Exploratory Behavior by Rat. Curr. Biol. *27*, 688–696.

47. Clarke, S., and Trowill, J.A. (1971). Sniffing and motivated behavior in the rat. Physiol. Behav. *6*, 49–52.

48. Ranade, S., Hangya, B., and Kepecs, A. (2013). Multiple Modes of Phase Locking between Sniffing and Whisking during Active Exploration. J. Neurosci. *33*, 8250–8256.

49. Kesner, A.J., Shin, R., Calva, C.B., Don, R.F., Junn, S., Potter, C.T., Ramsey, L.A., Abou-Elnaga, A.F., Cover, C.G., Wang, D.V., et al. (2021). Supramammillary neurons projecting to the septum regulate dopamine and motivation for environmental interaction in mice. Nat. Commun. *12*, 2811.

50. Hnasko, T.S., Hjelmstad, G.O., Fields, H.L., and Edwards, R.H. (2012). Ventral Tegmental Area Glutamate Neurons: Electrophysiological Properties and Projections. J. Neurosci. *32*, 15076–15085.

51. Margolis, E.B., Lock, H., Hjelmstad, G.O., and Fields, H.L. (2006). The ventral tegmental area revisited: is there an electrophysiological marker for dopaminergic neurons? J. Physiol. *577*, 907–924.

52. Faget, L., Osakada, F., Duan, J., Ressler, R., Johnson, A.B., Proudfoot, J.A., Yoo, J.H., Callaway, E.M., and Hnasko, T.S. (2016). Afferent Inputs to Neurotransmitter-Defined Cell Types in the Ventral Tegmental Area. Cell Rep. *15*, 2796–2808.

53. Chen, T.W., Wardill, T.J., Sun, Y., Pulver, S.R., Renninger, S.L., Baohan, A., Schreiter, E.R., Kerr, R.A., Orger, M.B., Jayaraman, V., et al. (2013). Ultrasensitive fluorescent proteins for imaging neuronal activity. Nature *499*, 295–300.

54. Chow, B.Y., Han, X., Dobry, A.S., Qian, X., Chuong, A.S., Li, M., Henninger, M.A., Belfort, G.M., Lin, Y., Monahan, P.E., et al. (2010). High-performance genetically targetable optical neural silencing by light-driven proton pumps. Nature *463*, 98–102.

55. Wu, A., Buchanan, E.K., Whiteway, M., Schartner, M., Meijer, G., Noel, J.-P., Rodriguez, E., Everett, C., Norovich, A., Schaffer, E., et al. (2020). Deep Graph Pose: a semi-supervised deep graphical model for improved animal pose tracking. In Advances in Neural Information Processing Systems (Curran Associates, Inc.), pp. 6040–6052.

56. Hu, X., Khanzada, S., Klütsch, D., Calegari, F., and Amin, H. (2022). Implementation of biohybrid olfactory bulb on a high-density CMOS-chip to reveal large-scale spatiotemporal circuit information, Biosens. Bioelectron *198*, 113834.

STAR★METHODS

KEY RESOURCES TABLE

REAGENT or RESOURCE	SOURCE	IDENTIFIER
Antibodies		
Anti-TH, rabbit polyclonal	Millipore	Cat.: #AB152; RRID: AB_390204
Anti-synapsin I-Cy5, mouse monoclonal prelabeled	SySy	Cat.: #106 011C5; RRID: AB_2619761
Anti-Bassoon, rabbit polyclonal	Custom-made	N/A
Anti-Shank3, guinea pig polyclonal antiserum	SySy	Cat.: #162304; RRID: AB_2619863
Donkey Anti-rabbit Alexa Fluor 405	Abcam	Cat.: #ab175649; RRID: AB_2715515
Donkey Anti-rabbit Alexa Fluor 594	Abcam	Cat.: #ab150076; RRID: AB_2782993
Goat Anti-guinea pig-Alexa Fluor 647	ThermoFisher Scientific	Cat.: #A-21450; RRID: AB_2535867
Bacterial and virus strains		
AAV1.Syn.Flex.GCaMP6s.WPRE.SV40	Chen et al.[53]	Addgene, Cat.: #100845
AAV1 or AAV9-EF1a-double floxed-hChR2 (H134R)-EYFP-WPRE-HGHpa	gift from Karl Deisseroth	Addgene, Cat.: #20298
AAV9-FLEX-Arch-GFP	Chow et al.[54]	Addgene, Cat.: #22222
AAV1-EF1a-DIO EYFP	gift from Karl Deisseroth	Addgene, Cat.: #27056
AAV1-FLEX-tdTomato	gift from Edward Boyden	Addgene, Cat.: #28306
AAV2.1-Ef1a-double floxed-hChR2 (H134R)-EYFP-WPR	Wu et al.[55]	Addgene, Cat.: #20940
Chemicals, peptides, and recombinant proteins		
TTX	Tocris	Cat.: #1069
4-AP	Sigma	Cat.: #A78403-25G
NBQX	Tocris	Cat.: #0373
D-AP5	Tocris	Cat.: #0106
Lidocaine	Sigma	Cat.: #L5647-15G
PFA	Sigma	Cat.: #158127-500G
NaCl	Sigma	Cat.: #S3014-1KG
Sucrose	Sigma	Cat.: #S0389-500G
KCl	Sigma	Cat.: #P9541-500G
NaHPO4	Sigma	Cat.: #S8282-500G
NaHCO3	Sigma	Cat.: #S5761-500G
CaCl2	Sigma	Cat.: #C5670-100G
MgCl2	Sigma	Cat.: #M2670-500G
MgSO4	Sigma	Cat.: #230391-1KG
Glucose	Sigma	Cat.: #G8270-1KG
K-gluconate	Sigma	Cat.: #G4500-100G
HEPES-acid	Sigma	Cat.: #H3375-250G
Phosphocreatine	Sigma	Cat.: #P7936-1G
EGTA	Sigma	Cat.: #E3889-10G
Biocytin	Sigma	Cat.: #B4261-25MG
Aqua-Poly/mount	Polysciences	Cat.: #18606-20
Normal Donkey Serum (NDS)	Jackson	Cat.: #017-000-121
Triton X 100	Roth	Cat.: #3051.4
Experimental models: Organisms/strains		
Mouse: Vglut2-ires-cre/Slc17a6$^{tm2(cre)Lowl}$/J	The Jackson Lab	Strain #: 016963; RRID:IMSR_JAX:016963

(*Continued on next page*)

Continued

REAGENT or RESOURCE	SOURCE	IDENTIFIER
Software and algorithms		
Pylon Viewer	Basler	https://www2.baslerweb.com/en/downloads/software-downloads/
IGOR Pro	WaveMetrics	RRID: SCR_000325
Prism	GraphPad	RRID: SCR_002798
DeepLabCut	Mathis et al.[26]	https://github.com/DeepLabCut
VAME	Luxem et al.[28]	https://github.com/LINCellularNeuroscience/VAME
DeepGraphPose	Wu et al.[55]	https://github.com/paninski-lab/deepgraphpose
MouseFlow	Barnstedt et al.[27]	https://github.com/obarnstedt/MouseFlow
Custom written MATLAB code	this article	https://doi.org/10.5281/zenodo.10407377
Custom written Python code	this article	https://doi.org/10.5281/zenodo.10406017
OpenCV library	OpenCV	RRID: SCR_015526
Elephant library	Elephant	RRID: SCR_003833
Scipy library	Scipy	RRID: SCR_008058
Scikit-learn library	Scikit-learn	RRID: SCR_002577
Imaris	Bitplane	RRID: SCR_007370
Huygens Professional	Scientific Volume Imaging	RRID: SCR_014237
Fiji/ImageJ	NIH	RRID: SCR_002285; SCR_003070
MATLAB	Mathworks	RRID: SCR_000325
Python	Python	RRID: SCR_008394
Other		
NI board	National Instruments	NI USB-6009
Fiberphotometry system	NPI Electronic	https://www.npielectronic.com/product/fiberoptometer/

RESOURCE AVAILABILITY

Lead contact

Further information and requests for resources, reagents, and code should be addressed to and will be fulfilled by the Lead Contact, Stefan Remy (Stefan.Remy@lin-magdeburg.de).

Materials availability

This study did not generate new unique reagents.

Data and code availability

- All data reported in this paper will be shared by the lead contact upon request.
- All original code has been deposited at Zenodo and is publicly available as of the date of publication. DOIs are listed in the key resources table.
- Any additional information required to reanalyze the data reported in this paper is available from the lead contact upon request.

EXPERIMENTAL MODEL AND STUDY PARTICIPANT DETAILS

All experiments were performed in adult male and female VGluT2-cre mice. The transgenic mice (Slc17a6tm2(cre)Lowl/J, stock number 016963, Jackson Lab, Bar Harbor, USA) were bred under specific pathogen-free conditions. Heterozygous mice were group-housed with 12 hours reversed dark-light cycle at 21°C and *ad libitum* access to food and water. Experiments were performed during the dark phase. All experiments were performed according to the Directive of the European Communities Parliament and Council on the protection of animals used for scientific purposes (2010/63/EU) and were approved by the animal care committee of North Rhine-Westphalia and Sachsen-Anhalt, Germany.

METHOD DETAILS

Stereotactic viral injection

The mice were anesthetized with an intraperitoneal (i.p.) injection of ketamine (0.13 mg/g) and xylazine (0.01 mg/g) and warmed with a 37°C heating pad (Fine Science Tools) for the entire length of the procedure. The animals were head-fixed using a non-punctuated head bar and a nose clamp (MA-6N, Narishige), and placed under a motorized stereotactic frame (Luigs-Neumann). An incision was made in the scalp, and bregma and lambda were measured to ensure the skull was horizontally aligned. A small craniotomy was performed on top of the region of interest and a 34-gauge needle and Hamilton syringe (World Precision Instruments) were used for the injection. All coordinates were calculated using the Allen Mouse Brain Atlas as a reference. For the stereotactic MSDB injections the coordinates were +1 mm anterior-posterior, -0.75 mm lateral, and -4.3 mm ventral relative to bregma with a 10° angle. All viruses were injected using an UltraMicroPump (World Precision Instruments). For fiber photometry experiments 500 nl of a genetically encoded calcium indicator (AAV1.Syn.Flex.GCaMP6s.WPRE.SV40, Addgene catalog number 100845, Chen et al.[53]) was injected in the MSDB at a speed of 100 nl/min. For *in vivo* optogenetic experiments 200 nl of channelrhodopsin virus (AAV1 or AAV9-EF1a-double flozed-hChR2(H134R)-EYFP-WPRE-HGHpa, Addgene catalog number 20298), archaerhodopsin (AAV9-FLEX-Arch-GFP, Addgene catalog number 22222, Chow et al.[54]) or control virus (AAV1-EF1a-DIO-EYFP, Addgene catalog number 27056) was injected in the MSDB at 100 nl/min. For slice patching experiments 500 nl of AAV2.1-Ef1a-double floxed-hChR2(H134R)-EYFP-WPR (Addgene catalog number 20940, Chow et al.[54]) was injected at 2 different depths (-4.6 mm and -4.2 mm) at a speed of 100 nl/min into the MSDB. After all injections the needle was left in place for at least 5 minutes before withdrawal. The scalp was then sutured, and the animals were injected i.p. with buprenorphine (0.05 mg/kg) twice daily for 3 days. Once the experiments were concluded all mice were transcardially perfused, first with PBS, followed by 4% PFA in PBS. The brain was removed and stored in 4% PFA in PBS for at least 24 hours. Afterwards, the brain tissue was sliced, and the viral expression was confirmed under a confocal microscope.

Chronic surgery

As described before, mice were anesthetized and placed in the stereotactic frame. In addition, they received an i.p. injection of dexamethasone (0.2 mg/kg) and carprofen (5 mg/kg) before surgery. Dental acrylic (Cyano-Veneer fast; Heinrich Schein Dental Depot) served to fix all the implants. For head-fixed experiments, a small metal bar was placed on the skull paramedially. After surgery, the mice received an i.p. buprenorphine injection for 3 days twice a day. The mice were allowed to recover for at least 2 weeks before starting the behavioral tests.

Behavioral tests

Before any behavioral test, mice were handled by the experimenter for a week. For head-fixed experiments, the animals were habituated for at least 1 week to the experimental room and the head-fixation. For freely moving experiments, the animals were habituated to the room for a week before starting the experiments.

Head-fixed experiments

For head-fixed experiments the mice were running on a 7 cm wide, 3.6 m long linear treadmill (Luigs & Neumann). The rotation of the belt (and thus the movement of the animal) is detected with a rotary encoder and computed into a virtual position change. In addition, the actual position of the treadmill is checked using a reflection light barrier and the virtual position is corrected accordingly. The signal was collected at 10 kHz by an I/O board (USB-6212BNC, National Instruments, Austin, USA) and recorded using custom-written Python software. Head-fixed mouse behavior was continuously monitored by simultaneously using two monochrome CCD cameras (Basler acA 780-75gm) positioned at approximately 15 cm from the mouse. To capture face dynamics, we used a high-resolution zoom lens (50 mm FL, Thorlabs MVL50TM23); for body dynamics, we used a wide-angle lens (12 mm FL, Edmund Optics #33-303). Infrared illumination was provided via two 850 nm LED arrays (Thorlabs LIU850A), and cameras were outfitted with 780 nm longpass filters (Thorlabs FGL780). Both cameras' positions were aligned for each mouse before the start of recordings. Camera images were acquired at 75 Hz with 782×582 pixels using pylon Camera Software Suite (Basler), each frame triggered by TTL pulses from the recording software. Files were saved in compressed MP4 format before further processing.

Head-fixed reward learning task

Two weeks before performing the reward learning task, mice were subjected to food restriction. They received 80% of their usual consumption of food pellets every 24 hours. The animals were monitored so that their weight was kept constant and never exceeded more than 10% loss of their initial body weight. During the habituation period, mice were exposed by the experimenter to high-fat milk that they could receive from a metal cannula at the end of each handling session. The same treadmill apparatus described above was used. The only difference was the enrichment of the belt with six different textures of 60 cm each for precise spatial indications of where the reward would be delivered. The reward consisted of high-fat milk that the mice could receive from a metal cannula spout placed in front of their mouths. In the first 6-8 days all mice learnt to run on the new cued belt and received the milk reward every time they crossed the reward zone. Reward delivery was automated with custom-written Python code, which activated a peristaltic pump whenever the animal's position matched the defined reward position (90-180 cm from the beginning of the belt). After mice had

learned to lick at the reward position, a threshold was introduced for the mice to receive the reward. Only when the licking activity at the correct reward position was performed did the pump activate and the animal could collect the reward. Once all mice had learnt to lick in the reward location, optogenetic stimulation was introduced. The mice received optogenetic stimulation at 9 Hz before and at the reward zone (60-180 cm). Two days later, a second stimulation zone was introduced 180 cm from the first (240-300 cm).

Open field

Unless otherwise specified, the open field experiments were performed in a 50 cm wide circular arena made of transparent plexiglass. The arena was located in a custom-built metal structure with black curtains all around and a transparent floor at 1 meter height from the ground made of 1 cm transparent plexiglass and 3 mm red plexiglass on top. Four infrared lights (LIU780A, Thorlabs) were placed at the 4 edges of the arena to homogeneously illuminate the area from below. The animals were recorded with a bottom-view CMOS camera (Basler acA2040-90umNIR) located at the center of the arena, 70 cm away from it. In a subset of experiments, the animals were exposed to novel stimuli, one stimulus per day (a novel object of around 6×6 cm, novel food in the form of chocolate chips, or a novel mouse with matched age and sex). All recordings were performed in darkness.

Open field anxiety test

For the anxiety test a 70 cm wide cardboard arena was used. A top-view camera (Basler acA2040-90umNIR) recorded the animal's position throughout the experiment. A bright light illuminated the center of the arena. A lux meter (MS 1300, Voltcraft) was used to measure the light intensity in the middle (200 Lux) and at the walls (5 to 10 Lux) of the arena.

Elevated plus maze (EPM) test

A custom-built EPM was used in these experiments. Each arm measured 30 cm in length, the corridors were 5 cm wide and the walls 15 cm high. The experimental room was illuminated with white light and the animals were placed in the centre of the maze and tested for 10 minutes each. Optogenetic stimulation (9 Hz for $MSDB_{glu}$-VTA:ChR mice and 0.1 Hz for $MSDB_{glu}$-VTA:Arch mice) was spatially triggered by the animal's position in the enclosed arm of the maze via a custom-written Python code.

Fiber photometry recordings

For fiber photometry experiments, a fiber-optic cannula (MFC_400/430-0.37_5mm_SM3(P)_FLT, Doric Lenses) was implanted unilaterally on top of VTA (coordinates: -3.3 mm anterior-posterior, -0.4 mm lateral, -4 mm ventral, relative to bregma). A FiberOptoMeter (npi electronics) was used to perform the fiber photometry recordings. The 470 nm diode was collimated into a fiber-optic patch-cord (MFP_400/430/1100_0.37_1m_FC_CM3(P), Doric Lenses). The light intensity at the fiber tip was 0.6 to 1.2 mW. The signal was converted into an analog voltage signal, sampled at 10 kHz using an ITC-18 interface (HEKA Elektronik) and recorded with a custom-written Igor Pro 6.3 software (WaveMetrics).

Optogenetic recordings

For optogenetic experiments in head-fixed and freely moving conditions, a fiber-optic cannula (DFC_200/245-0.37_5mm_GS1.0_FLT, Doric Lenses, Quebec, Canada) was implanted bilaterally on top of VTA (coordinates: -3.3 mm anterior-posterior, -0.4mm lateral, -4 mm ventral, relative to bregma). Light stimulation was performed with a fiber-coupled 473 nm diode laser (LuxX 473-80, Omicron-Laserage) for optogenetic excitation or a 561 nm laser (OBIS 561-80 LS FP, COHERENT, Santa Clara, CA, USA) for optogenetic inhibition. For the optogenetic excitation, the square pulse TTL signal at 3, 6, 9, or 12 Hz was generated via custom-written Igor Pro 6.3 software (WaveMetrics) to modulate the laser output. The square pulse width was adjusted based on the frequency of the stimulation to guarantee a constant total time of illumination: 50 ms at 3 Hz, 25 ms at 6 Hz, 16 ms at 9 Hz, and 12 ms at 12 Hz. The length of each stimulation epoch is of 20 s with 20 s pre-stimulation and 20 s post-stimulation epochs, unless otherwise specified. For the optogenetic inhibition, a TTL signal of 0.1 Hz was generated via custom-written Igor Pro 6.3 software (WaveMetrics) to modulate the laser output.

Pharmacological manipulation

For treadmill experiments, animals had a small craniotomy on top of the MSDB (+1 mm anterior-posterior, -0.75 mm lateral relative to bregma) sealed with Kwik-Cast (World Precision Instruments). On the day of the experiment, mice were head-fixed on the treadmill, the sealant was removed, and lidocaine was acutely injected with a 34-gauge cannula and Hamilton syringe (World Precision Instruments) using a UltraMicroPump (-4.3 mm ventral relative to bregma with a 10° angle). The UltraMicroPump connected to a plastic tube to the internal cannula was used for drug injection. All mice were injected with 500 nl of lidocaine (40 mg/ml in cortex buffer) delivered at 100 nl/min. After injections, mice were given 15 minutes to recover and to let the drug diffuse in the brain before the start of recordings. The silencing efficiency was evaluated by comparing hippocampal LFP amplitude before and after the perfusion of the drug. For open field experiments, mice were implanted with an infusion cannula (guide: C315GS-5-SP 388834 26GA 5MM PED, CUT 4 mm, dummy: C315DCS-5-SPC SM.008-.2mm, FIT 4mm C315GS-S W0 PROJ, internal: C315IS-5-SPC 33GA FIT 5mm PED GUIDE, FIT 4mm C315GS-5 W 1mm PROJ, P1 Technologies, Virginia, USA) for drug delivery in the MSDB (anterior-posterior: +1 mm, lateral: -0.7, ventral: -3.5, relative to bregma with a 10° angle).

LFP recordings

To record hippocampal local field potentials, a monopolar tungsten electrode (W558511, Advent Research Materials) was positioned in the hippocampus. The coordinates were: -2 mm anterior-posterior, +2 mm lateral, -1.6 mm ventral relative to bregma. Reference and ground electrodes were placed on top of the cerebellum. The LFP was recorded using an extracellular amplifier (EXT-02F/2, npi electronic), sampled at 25 kHz using an ITC-18 interface (HEKA Elektronik) and recorded with a custom-written Igor Pro software (WaveMetrics).

Electrophysiological recordings in brain slices

Four to six weeks after virus injection, mice were deeply anesthetized and decapitated. The preparation of coronal VTA brain slices was performed with a VT-1200S vibratome (Leica Microsystems, Wetzlar, Germany) with standard solutions as described in Fuhrmann et al.[7] Current-clamp whole cell recordings were performed at 35°C ± 1°C (Heated Perfusion Tube, ALA scientific) using a Dagan BVC-700A amplifier and digitalized at 25 kHz using an ITC-18 interface board (HEKA Elektronik) controlled by IgorPro 6.3 software (WaveMetrics). Recording pipettes were pulled with a horizontal puller (DMZ-Universal Puller) to a resistance of 3-6 MΩ. The recording pipettes were filled with standard intracellular solution ([mM]: 140 K-gluconate, 7 KCl, 5 HEPES-acid, 0.5 $MgCl_2$, 5 phosphocreatine, 0.16 EGTA (pH: 7.3, osmolarity: 289 mOsm)). Biocytin (0.4%) was added freshly before the recording to subsequently localize and reconstruct the patched neurons. Whole-cell current-clamp recordings of VTA neurons were performed and the resting membrane potential was annotated immediately after the whole-cell formation. The series resistance for the cell recordings was between 13 and 55 MΩ (29.9 ± 9.8 mean series resistance ± s.d.). Neuronal membrane potential was kept between -65 and -60 mV. For electrophysiological characterization, a series of hyperpolarizing and depolarizing step current injections lasting 500 ms each was performed with the following amplitudes: −200 pA, −100 pA, −50 pA, −30 pA, −20 pA, −10 pA, +10 pA, +20 pA, +30 pA, +50 pA, +100 pA, +200 pA, +300 pA, +400 pA and +500-pA. Optogenetic stimulation of $VGluT2^+$ ChR^+ MSDB axons was performed with a light fiber coupled 473 nm diode laser (LuxX 473-80, Omicron-Laserage), placed at around 5 mm distance from the slice, and activated at theta-band frequencies (3, 6, 9 and 12 Hz) for 1 s with 3-ms light pulses. If VTA neurons exhibited PSPs in control conditions with aCSF, the same optogenetic stimulation was performed after bath application of TTX (1 μM) and 4-AP (100 μM) to confirm the monosynaptic nature of the input, followed by NBQX (10 μM) and D-AP5 (50 μM) application to confirm its glutamatergic origin. After recording, the slices were kept in 4% PFA overnight and then washed and conserved in PBS.

Multielectrode array (MEA) recordings

MSDB coronal slices were prepared according to the procedure described by Hu et al.[56] The recording aCSF solution was modified as follows, in [mM]: 127 NaCl, 2.5 KCl, 1.25 NaH2PO4, 24 NaHCO3, 25 Glucose, 1.25 MgSO4, 2.5 CaCl2. MEA recordings were performed using a CMOS-based high density MEA system (MaxOne, MaxWell Biosystems, Zurich, Switzerland). After recovery for at least 1 hour at room temperature, a slice was placed on the CMOS chip and held with a handmade grid. During recording, the slice was constantly perfused with recording aCSF at 37°C. For light stimulation, the end of an optical fiber connected to an 80 mW 561 nm laser, OBIS 561-80 LS FP (Coherent, Santa Clara, CA, USA) was placed approximately 10 mm above the slice surface. Approximately one thousands of recording channels were selected and placed over the MSDB area. Only the channels showing significant single units were analyzed.

Antibody staining

Slices of 300 μm thickness were fixed in 4% PFA solution overnight and then washed three times in PBS (0.1M) for 10 minutes each. Non-specific antibody binding was prevented by incubating for 1 hour at room temperature with a PBS-based blocking solution of 10% NDS and 1% Triton-X-100. The primary antibody anti-TH (1:500) was incubated for 16 hours at 4°C in PBS with 1% NDS and 0.5% Triton-X-100. After 4 times 5 minutes washing in PBS, slices were incubated with the secondary antibody (Alexa Fluor 405) and streptavidin (Alexa Fluor 647) in 0.5% Triton X-100 PBS for 2 hours at room temperature. To remove the unbound secondary antibodies, slices were washed 6 times for 5 minutes each in PBS. Finally, they were mounted with Aqua-Poly/Mount and images were acquired using a confocal microscope (LSM700, Zeiss, Germany) with a 20× objective (Plan-Apochromat 20×/0.8, Zeiss, Germany). The post-hoc validation of virus injection and implants for the *in vivo* experiments followed a similar procedure except that the slice thickness was 100 μm. For some experiments an additional DAPI staining was performed.

For the assessment of anatomical connectivity between MSDB and VTA, knockin mice expressing Cre recombinase under the control of the Slc17a6 locus (vesicular glutamate transporter; Vglut2-ires-cre/Slc17a6tm2(cre)Lowl/J) were injected with AAV particles expressing EYFP in excitatory neurons of the MSDB (AAV1-EF1a-DIO-EYFP) as well as tdTomato in the excitatory neurons in the VTA (AAV1-FLEX-tdTomato) as described above. Four to five weeks post-injection, animals were perfused, their brains were dissected, and 40 μm slices were obtained from cryostat slicing. Brain sections were permeabilized with 0.2% Triton X100 in PBS for 1 hour, washed with 1xPBS, and incubated for at least 2 hours in a blocking buffer (2% glycine, 0.2% gelatin, 2% BSA, and 50 mM NH3Cl (pH 7.4) containing 0.1% Triton X100. Primary antibodies were diluted in the blocking buffer (200 μl/per slice) and incubated at 4°C on a shaker for 72 h. For immunohistochemical detection of dopaminergic (DA) neurons and DA neurons co-releasing glutamate, anti-tyrosine hydroxylase (TH, Millipore) antibodies were co-applied with pre-labelled KO-verified mouse monoclonal anti-synapsin I-Cy5 antibodies (SySy) detecting synaptic vesicles available for release. For the assessment of excitatory synapses between MSDB terminals and VGluT2-positive neurons, antibodies raised against major scaffolding protein at the

cytomatrix of the active zone, Bassoon (custom-mage rabbit polyclonal), and postsynaptic protein Shank3 (guinea pig polyclonal antiserum, SySy) were used. Subsequently, sections were washed 3× times in 1X PBS and incubated with donkey anti-rabbit Alexa Fluor 405 and goat anti-guinea pig-AlexaFluor 647 secondary antibodies accordingly for 2 hours. After additional washing steps, brain sections were mounted with Mowiol 4-88 (Calbiochem), and images were acquired either with 63×/1.4Oil (HC Pl APO SC2 63×/NA1.4Oil, Leica) or 100×/1.4Oil (HC PL APO CS2 100×/1.4Oil, Leica) objectives along the z-axis with 200 nm z-step in 1024 × 1024-pixel formats at 8-bit image depth with at least two times frame average at 400 Hz laser frequency using the Leica SP8 3X STED LCM system (Leica-Microsystems, Mannheim, Germany) equipped with a white light laser (WLL). Raw confocal images were deconvolved using the Deconvolution wizard (Huygens Professional, Scientific Volume Imaging, The Netherlands, http://svi.nl). Subsequently, images were rendered in 3D using Imaris software (Bitplane). Mainly, EYFP and tdTomato cell fill was used to create an isosurface that was applied to mask synapsin I-Cy5 staining, as well as Bassoon and Shank3 accordingly.

QUANTIFICATION AND STATISTICAL ANALYSIS

Data analysis

Detection and analysis of movement

To consider a locomotor epoch valid the mouse had to move at a speed of at least 2 cm/s for 2 seconds with 1 second of immobility before. Movement onset is calculated as the first time the speed overcomes 0.5 cm/s on the treadmill experiments. For freely moving data we used the average *x* and *y* position of the pose estimation data (see pose estimation and behavioral quantification paragraph for additional details) to calculate distance, mean speed, and max speed and time spent moving.

Treadmill camera recordings analysis

All analyses were performed either in Python or R. Markerless pose estimation (DeepGraphPose/DeepLabCut Mathis et al.[26]; Wu et al.[55]) was used to detect facial movements. For this, a deep neural network was trained to automatically discriminate 13 markers for videos of the face (6 for pupil, eye, nose, mouth, etc). The network was trained on a large variety of lighting conditions and angles until it reached satisfactory performance. Whisker pad and nose facial regions of interest were automatically segmented using video-averaged marker points of nose tip, the eye's tear duct and the mouth as stable landmarks.

Dense optical flow of face regions was calculated using Python-based OpenCV (v4.2) *cuda_FarnebackOpticalFlow* function and averaging frame-to-frame optical flow magnitude and angle per facial region.[27] Optical flow magnitude was then Z-scored by subtracting the mean and dividing by the standard deviation from the entire time series.

Fiber photometry analysis

Fiber photometry data were first downsampled to 1 kHz. A third-degree polynomial function was fitted to the original signal. The resulting polynomial values were then subtracted to the signal along the time axes in order to detrend it (detrended signal = d_signal). The ΔF/F was calculated as d_signal/min(d_signal) and smoothed only for visualization purposes. The Z-score was calculated as (ΔF/F)/standard deviation (ΔF/F) in order to compare the signal between animals.

Analysis of hippocampal local field potentials

First, we removed the 50 Hz noise from the hippocampal local field potentials using a notch filter (scipy.signal.iirnotch). Further, we applied a Hilbert function (scipy.signal.hilbert) to calculate the signal envelope and use it to exclude fast, high frequency artifacts with a custom written despike function. The signal was then processed with a butterworth bandpass filter (2 and 15 Hz). To calculate the spectrogram we used the Morlet wavelet transform over 9 cycles (elephant.signal_processing.wavelet_transform). Welch's method was used to estimate the power spectral density (elephant.spectral.welch_psd) and calculate the maximum power for each frequency in the theta range.

Pose estimation and behavioral quantification

Mice pose estimation from the 40Hz bottom-up view videos were extracted using DeepLabCut.[26] 20 frames per video were manually annotated selecting 6 points of the mouse body (nose, right front paw, left front paw, right hindpaw, left hindpaw, tail base). The network (ResNet-50) was trained up to 10^6 iterations and DeepLabCut pose tracking results were saved. The approaches time in the open field novel cue test were counted whenever the line drawn from the coordinates of the mouse's tail to the nose intersected the centrally positioned cue and the mouse was within 10 cm from the cue. The head dippings in the EPM were calculated based on the position of the mouse's nose. VAME,[26] a self-supervised method for behavioral quantification, allowed to identify behavioral motifs starting from the DLC files. After training VAME on the freely moving data, we identified the relevant number of motifs by first segmenting the data into 100 motifs and then considering only the motifs that overcome the 1% usage threshold. This resulted in the identification of 35 distinct behavioral motifs. Afterwards, we determined the communities as groups of highly connected motifs by creating a hierarchical tree representation of the Markovian time series. After visual inspections of the single motif videos and the hierarchical representation, six communities were identified describing well-defined behavioral actions.

Community glossary

VAME is assigning a motif number to each frame that is further categorized into communities. The community behavioral representation was defined by observing the videos (as the one provided in Video S2) and identifying the most prominent actions performed by the mice referring to mousebehavior.org. Our definitions are described below:

a_Running: rapid locomotion in the center or around the arena (motifs #0, 2, 27, 29, 32)

b_Rearing: weight on hind legs, raise, forelimbs on the ground (motifs #3, 4, 7, 14, 25, 33)
c_walking: slow locomotion, when approaching the walls or before moving to another behavioral action (motifs #11, 17, 19, 20, 23, 28)
d_sniffing: nose held in the air (motifs #1, 5, 10, 18, 24)
e_grooming: sitting position, combination of lick, groom and scratch (motifs #6, 13, 15, 21)
f_resting: immobile sitting (motifs #8, 9, 16, 26, 30, 31)

Motifs 12, 22, 34 were detected in less than 5% of all the videos analyzed with a motifs usage <0.001 and were thus not taken into account for further analysis.

Analysis of in vitro *recordings*

For patch-clamp whole cell recordings, subthreshold, action potential and after-hyperpolarization properties of the neurons were quantified as in Justus et al.[11] Briefly, subthreshold properties were calculated based on the hyperpolarizing and depolarizing current injections that could not elicit action potentials (AP). Resting membrane potential, input resistance, membrane time constant (τ), sag index and rebound index were quantified. Firing properties and after-hyperpolarization properties were calculated based on the depolarizing current injections able to elicit at least one AP. AP threshold, half-width, amplitude, latency, and time to peak were quantified. Firing properties were measured from the current injection giving rise to the maximum number of APs. Firing frequency, amplitude and interspike interval were quantified. For MEA recordings, signals were high-pass filtered at 300 Hz and single units were detected by counting only those that exceeded five times the standard deviation of the signal. Only the channels showing significant single units were analyzed.

Cluster analysis

The electrophysiological values of the patched cells were transformed into principal components via principal component analysis (PCA). We calculated the cumulative variance and identified the number of principal components that explain 80% of the variance for our data. This resulted in 11 components that were afterwards used for clustering. Based on the Elbow method we identified 7 as the number of clusters that can optimally segregate our cells. We performed both k-means and agglomerative clustering and found that 5 clusters could better explain our cells' features.

Axonal fluorescence quantification

Confocal tile scan z-stack images were acquired using the Leica SP8 3X STED LCM system (Leica-Microsystems, Mannheim, Germany). Based on the Paxinos brain atlas, the different brain regions were hand-drawn in each image and the intensity of the fluorescent signal per volume was calculated using ImageJ/FIJI functions.

Statistical analysis

Statistical analysis was performed using Prism 10. Statistical tests are indicated in the figure legends. To evaluate statistical significance, data from Figures 1D, 2C, 2G, 2H, 5G, 5H, 5J, S3A, S4E, S7C, and S7J, were subjected to Student's t tests. Data from Figures 1G, 1J, 3B, 3C, 4C, 4F–4I, 5B–5D, S2C, S3C–S3F, S4C, S4D, S4F, S4G, S5C, S5G, S6B–S6D, and S7D were subjected to repeated measures (RM) one- or two-way ANOVAs followed by Sidak or Tukey post-hoc analysis. Data from Figures 4B and 4C were subjected to three-way ANOVA. Data from Figures 5G–5J were subjected to one-way ANOVA followed by Tukey's multiple comparison test. Kruskal-Wallis test was used for nonparametric data followed by Dunn's multiple comparisons test from Figures 6E and S9E–S9G. For all analyses data are presented as mean ± SEM unless noted, and the threshold for significance was at $p < 0.05$.